



## 1 Is water vapor a key player of the wintertime haze in North China Plain?

2  
3 Jiarui Wu<sup>1,4,7</sup>, Naifang Bei<sup>2</sup>, Bo Hu<sup>3</sup>, Suixin Liu<sup>1,4</sup>, Meng Zhou<sup>5</sup>, Qiyuan Wang<sup>1,4</sup>, Xia Li<sup>1,4,7</sup>, Lang Liu<sup>1,4,7</sup>, Tian  
4 Feng<sup>1</sup>, Zirui Liu<sup>3</sup>, Yichen Wang<sup>1</sup>, Junji Cao<sup>1,4</sup>, Xuexi Tie<sup>1,4</sup>, Jun Wang<sup>5</sup>, Luisa T. Molina<sup>6</sup>, and Guohui Li<sup>1,4\*</sup>5  
6 <sup>1</sup>Key Lab of Aerosol Chemistry and Physics, SKLLQG, Institute of Earth Environment, Chinese Academy of  
7 Sciences, Xi'an, Shaanxi, China8 <sup>2</sup>School of Human Settlements and Civil Engineering, Xi'an Jiaotong University, Xi'an, Shaanxi, China9 <sup>3</sup>State Key Laboratory of Atmospheric Boundary Layer Physics and Atmospheric Chemistry, Institute of  
10 Atmospheric Physics, Chinese Academy of Sciences, Beijing, 100029, China11 <sup>4</sup>CAS Center for Excellence in Quaternary Science and Global Change, Xi'an, China12 <sup>5</sup>Department of Chemical and Biochemical Engineering & Interdisciplinary Graduate Program in

13 Geo-Informatics, University of Iowa, Iowa City, Iowa, USA

14 <sup>6</sup>Molina Center for Energy and the Environment, La Jolla, California, USA15 <sup>7</sup>University of Chinese Academy of Science, Beijing, China16 \*Correspondence to: Guohui Li ([ligh@ieecas.cn](mailto:ligh@ieecas.cn))

17

18

19 **Abstract.** Water vapor has been proposed to amplify the severe haze pollution in China by  
20 enhancing the aerosol-radiation feedback (ARF). Observations have revealed that the  
21 near-surface PM<sub>2.5</sub> concentrations ([PM<sub>2.5</sub>]) generally exhibits an increasing trend with  
22 relative humidity (RH) in North China Plain (NCP) during 2015 wintertime, indicating that  
23 the aerosol liquid water (ALW) caused by hygroscopic growth could play an important role in  
24 the PM<sub>2.5</sub> formation and accumulation. Simulations during a persistent and heavy haze  
25 pollution episode from 05 December 2015 to 04 January 2016 in NCP were conducted using  
26 the WRF-CHEM model to comprehensively quantify contributions of the ALW effect to  
27 near-surface [PM<sub>2.5</sub>]. The WRF-CHEM model generally performs reasonably well in  
28 simulating the temporal variations of RH against measurements in NCP. The factor separation  
29 approach (FSA) was used to evaluate the contribution of the ALW effect on the ARF,  
30 photochemistry, and heterogeneous reactions to [PM<sub>2.5</sub>]. The ALW not only augments particle  
31 sizes to enhance aerosol backward scattering, but also increases the effective radius to favor  
32 aerosol forward scattering. The contribution of the ALW effect on the ARF and  
33 photochemistry to near-surface [PM<sub>2.5</sub>] is not significant, generally within 1.0 μg m<sup>-3</sup> on  
34 average in NCP during the episode. Serving as an excellent substrate for heterogeneous  
35 reactions, the ALW substantially enhances the secondary aerosol (SA) formation, with an  
36 average contribution of 71%, 10%, 26%, and 48% to near-surface sulfate, nitrate, ammonium,  
37 and secondary organic aerosol concentrations. Nevertheless, the SA enhancement due to the  
38 ALW decreases the aerosol optical depth and increases the effective radius to weaken the  
39 ARF, reducing near-surface primary aerosols. The contribution of the ALW total effect to  
40 near-surface [PM<sub>2.5</sub>] is 17.5% on average, which is overwhelmingly dominated by enhanced  
41 SA. Model sensitivities also show that when the RH is less than 80%, the ALW progressively



42 increases near-surface  $[PM_{2.5}]$ , but commences to decrease when the RH exceeding 80% due  
43 to the high occurrence frequencies of precipitation.

44

45

46

47

48



## 49 1 Introduction

50 Atmospheric aerosols or fine particle matters ( $PM_{2.5}$ ) influence the climate directly by  
51 scattering and absorbing the solar radiation, and indirectly by serving as cloud condensation  
52 nuclei and ice nuclei (Ackerman, 1977; Ackerman and Baker, 1977; Jacobson, 1998, 2002;  
53 Penner et al., 2001). Moreover, high levels of  $PM_{2.5}$  in the atmosphere also cause severe haze  
54 pollution, impairing visibility and exerting deleterious effect on ecological system and human  
55 health (Chan and Yao, 2008; Zhang et al., 2013; Kurokawa et al., 2013; Weinhold, 2008;  
56 Parrish and Zhu, 2009). In addition to anthropogenic emissions, the poor air quality is  
57 generally influenced by stagnant meteorological situations with weak winds and high relative  
58 humidity (RH) (Flocas et al., 2009; Quan et al., 2013; Zhang et al., 2014; Bei et al., 2016; Wu  
59 et al., 2017; Ding et al., 2017). RH, as an important meteorological factor in the atmosphere,  
60 considerably affects the formation, chemical composition, and physical properties of  
61 atmospheric aerosols (Seinfeld et al., 2001; Hallquist et al., 2009; Poulain, 2010; Nguyen et  
62 al., 2011).

63 As the main constituent in the atmosphere, water vapor directly participates in the  
64 atmospheric physical and chemical processes. Since many components of atmospheric  
65 aerosols are hygroscopic, they take up water as RH increases (Covert et al., 1972; Pilinis et  
66 al., 1989), thereby influencing the aerosol size distribution, chemical composition, mass  
67 concentration, and corresponding optical properties as well as radiative effects (Im et al.,  
68 2001; Carrico et al., 2003; Randles et al. 2004; Cheng et al., 2008). Wang et al. (2016) have  
69 indicated that the ratio of  $SO_4^{2-}$  to  $SO_2$  exhibits an exponential increase with RH. Tie et al.  
70 (2017) have shown that the sulfate, nitrate, and ammonium concentrations increase from 16  
71 to  $25 \mu g m^{-3}$ , 15 to  $23 \mu g m^{-3}$ , and 11 to  $17 \mu g m^{-3}$ , respectively, when RH increases from 60%  
72 to 80%. Field measurements in Beijing have demonstrated that the inorganic aerosol fraction  
73 increases with increasing RH (Wu et al., 2018). In addition, water vapor also serves as an



74 important medium in the formation of secondary aerosols (SA) through liquid-phase  
75 reactions and heterogeneous reactions (Seinfeld and Pandis, 1986; Pilinis et al., 1989). For  
76 example, Li et al. (2017) have indicated that the aerosol liquid water (ALW) induced by the  
77 wet growth could play a significant role in the sulfate formation and emphasized the  
78 importance of bulk aqueous-phase oxidation of SO<sub>2</sub> in ALW and heterogeneous reaction of  
79 SO<sub>2</sub> on aerosol surfaces involving ALW. ALW also plays an important role in secondary  
80 organic aerosol (SOA) formation (Hastings et al., 2005; Healy et al., 2009; Kamens et al.,  
81 2011; Koehler et al., 2004). Numerous studies have investigated the effect of RH on SOA  
82 formed from different aromatics during their photochemical oxidation processes (Blando and  
83 Turpin, 2000; Cocker et al., 2001; Seinfeld et al., 2001; Zhou et al., 2011; Jia and Xu., 2014).  
84 Furthermore, Zhang et al. (2015) have revealed that, as the RH increases from 40% to 85% in  
85 the Yangtze River Delta of China, the aerosol scattering and backscattering coefficients  
86 increase by 58% and 25%, respectively, and the calculated aerosol direct radiative forcing  
87 caused by hygroscopic growth is increased by 47%.

88 In recent years, China has experienced persistent haze pollution with unprecedentedly  
89 high PM<sub>2.5</sub> concentrations during wintertime, particularly in North China Plain (NCP) (Chan  
90 and Yao, 2008; He et al., 2001; Kan et al., 2012; Guo et al., 2014; Wang et al., 2014; Fu et al.,  
91 2014). A conceptual model based on the aerosol radiation feedback (ARF) has been  
92 established to interpret the wintertime heavy haze formation, in which water vapor is  
93 considered to play a key role in the progressive accumulation and formation of PM<sub>2.5</sub>. In  
94 winter, when the atmospheric condition is stagnant, air pollutants commence to accumulate in  
95 the planetary boundary layer (PBL), favorable for the PM<sub>2.5</sub> formation. Increasing PM<sub>2.5</sub>  
96 scatters or absorbs the incoming solar radiation to lower the surface temperature and cause  
97 anomalous temperature inversion, subsequently suppressing the vertical turbulent diffusion  
98 and decreasing the planetary boundary layer height (PBLH) to further trap more air pollutants



99 and water vapor to increase the RH in the PBL. Increasing RH enhances aerosol hygroscopic  
100 growth and multiphase reactions and augments the particle size and mass, causing further  
101 dimming and decrease of the surface temperature and PBL height (Quan et al., 2013; Tie et  
102 al., 2017; Ding et al., 2017). However, few studies have been performed in China to  
103 comprehensively quantify the effect of water vapor in the atmospheric physical and chemical  
104 process on the PM<sub>2.5</sub> pollution to further verify the haze formation.

105 The purpose of the present study is to quantitatively evaluate the contribution of aerosol  
106 water induced by the aerosol wet growth to PM<sub>2.5</sub> concentrations in NCP using the Weather  
107 Research and Forecast model with Chemistry (WRF-CHEM). The model configuration and  
108 methodology are described in Section 2. Results and discussions are presented in Section 3,  
109 and conclusions and summaries are given in Section 4.

110

## 111 2 Model and methodology

### 112 2.1 WRF-CHEM Model and Configuration

113 A persistent air pollution episode with high levels of PM<sub>2.5</sub> from 05 December 2015 to  
114 04 January 2016 in NCP was simulated using the WRF-CHEM model with modifications by  
115 Li et al. (2010, 2011a, b, 2012) from the Molina Center for Energy and the Environment.  
116 Figure 1 shows the WRF-CHEM model simulation domain and Table 1 provides the model  
117 configurations. Detailed model description can be found in Wu et al. (2018a).

### 118 2.2 Data and Methodology

119 The model performance of RH was validated using the hourly measurements in  
120 Luancheng, Yucheng, and Jiaozhouwan observed from the Chinese Ecosystem Research  
121 Network (CERN). Furthermore, the NCEP reanalysis data was used to compare to the  
122 simulated RH distribution. The detailed information of other data used for validation can be  
123 found in Wu et al. (2018a).



124 The mean bias ( $MB$ ), root mean square error ( $RMSE$ ) and the index of agreement ( $IOA$ )  
125 were utilized to evaluate the performance of the WRF-CHEM model simulations against  
126 measurements. To assess the contributions of ALW to the near-surface concentrations of air  
127 pollutants in NCP, the factor separation approach (FSA) was used in this study (Stein and  
128 Alpert, 1993; Gabusi et al., 2008; Li et al., 2014). Generally, the formation of the secondary  
129 atmospheric pollutants, such as  $O_3$ , secondary organic aerosol, and nitrate, is a complicated  
130 nonlinear process in which its precursors from various emissions sources and transport react  
131 chemically or reach equilibrium thermodynamically. Nevertheless, it is not straightforward to  
132 evaluate the contributions from different factors in a nonlinear process (Wu et al., 2017). The  
133 factor separation approach (FSA) proposed by Stein and Alpert (1993) can be used to isolate  
134 the effect of one single factor from a nonlinear process and has been widely used to evaluate  
135 source effects. The total effect of one factor in the presence of others can be decomposed into  
136 contributions from the factor and that from the interactions of all those factors. Considering  
137 that there are two factors  $X$  and  $Y$  that influence the formation of secondary pollutants in the  
138 atmosphere and also interact with each other. Denoting  $f_{XY}$ ,  $f_X$ ,  $f_Y$ , and  $f_0$  as the  
139 simulations including both of two factors, factor  $X$  only, factor  $Y$  only, and none of the two  
140 factors, respectively. The contributions of factor  $X$  and  $Y$  can be defined as  $f_{XY} - f_Y$  and  
141  $f_{XY} - f_X$ , respectively. Detailed description of the methodology can be found in Wu et al.  
142 (2017).

143

### 144 3 Results and discussions

#### 145 3.1 Relationship between RH and near-surface $PM_{2.5}$ concentrations

146 High RH has been suggested to be an important factor facilitating the SA formation in  
147 the atmosphere and aggravating the haze pollution (Sun et al., 2013; Cheng et al., 2015).  
148 Figure 2 presents the scatter plot of the near-surface  $PM_{2.5}$  concentrations ( $[PM_{2.5}]$ ) and RH in



149 the winter of 2015 at six typical polluted cities in NCP, including Beijing, Tianjin,  
150 Shijiazhuang, Tangshan, Baoding, and Chengde. The observed near-surface  $[PM_{2.5}]$  at those  
151 six cities display a growing trend with increasing RH, suggesting that the ALW induced by  
152 the hygroscopic growth under high RH conditions has potentials to accelerate the  $PM_{2.5}$   
153 formation and accumulation. Increasing RH facilitates the aerosol hygroscopic growth and  
154 further enhances the ALW, which serves as an efficient medium for promoting the  
155 liquid-phase and heterogeneous reactions and accelerating the transformation of reactive  
156 gaseous pollutants into the particle phase. Increased ALW also augments the particle size,  
157 enhancing the ARF to increase the near-surface  $[PM_{2.5}]$ . However, the attenuation of  
158 incoming solar radiation caused by the ALW also decreases the photolysis rates, unfavorable  
159 for photochemical activities and lowering the atmospheric oxidation capability (AOC). Field  
160 measurements show that large fraction of SA in  $PM_{2.5}$  has been observed in NCP during  
161 wintertime (Sun et al., 2013; Guo et al., 2014; Xu et al., 2015). Therefore, decreased AOC  
162 generally does not facilitate the SA formation, particularly with regards to SOA and nitrate, to  
163 partially counteract the  $PM_{2.5}$  enhancement caused by the ALW. It is also worth noting that  
164 since high RH frequently corresponds to atmospheric stagnation, near-surface  $[PM_{2.5}]$  also  
165 build up under high RH conditions. For example, the humid air mass is subject to being  
166 transported from south to NCP under the stagnant weather with weak south winds and  
167 meanwhile the  $PM_{2.5}$  also accumulates due to the unfavorable dispersion condition.  
168 Additionally, when the RH is very high, there also exist the low near-surface  $[PM_{2.5}]$  shown  
169 in Figure 2, demonstrating that other factors, such as emissions, horizontal transport, vertical  
170 exchange, and precipitation, also substantially influence near-surface  $[PM_{2.5}]$ . Generally, high  
171 occurrence frequency of precipitation coincides with high RH, thus the precipitation washout  
172 might constitute one of the most possible reasons for the low near-surface  $[PM_{2.5}]$  under high  
173 RH situations. Therefore, it is still imperative to verify quantitatively the contribution of the



174 ALW to near-surface [ $\text{PM}_{2.5}$ ].

### 175 3.2 Model validation

176 The WRF-CHEM model simulation of the haze pollution episode in NCP has been  
177 comprehensively validated using available measurements in Wu et al. (2018a). In general, the  
178 model simulates well the spatial distribution and temporal variation of  $\text{PM}_{2.5}$ ,  $\text{O}_3$ ,  $\text{NO}_2$ ,  $\text{SO}_2$   
179 and CO mass concentrations compared to observations in NCP. The predicted aerosol species  
180 are also in good agreement with the measurement in Beijing. Moreover, the model performs  
181 reasonably well in simulating the aerosol optical depth and single scattering albedo, PBL  
182 height and downward shortwave flux against measurements.

183 In order to verify the effect of the ALW on near-surface [ $\text{PM}_{2.5}$ ] during the haze  
184 pollution episode, the simulated temporal variation of RH was first compared to  
185 measurements at Luancheng, Yucheng, and Jiaozhouwan in NCP from 05 December 2015 to  
186 04 January 2016 (Figure 3). The WRF-CHEM model generally performs well in simulating  
187 the hourly variation of RH in these three cities, with *IOAs* of 0.73, 0.83, and 0.69,  
188 respectively. RH is a key meteorological component, sensitive to the atmospheric  
189 thermodynamic (e.g., temperature) and dynamic (e.g., winds) conditions. Even when the  
190 simulated water vapor content is the same as the observation, the overestimation or  
191 underestimation of temperature still causes underestimation or overestimation of RH. Biases  
192 of wind speeds and directions considerably influence the origination of air mass at the  
193 observation site. In general, the northerly wind carries dry air, and is opposite for the  
194 southerly wind during wintertime in NCP. Therefore, the uncertainties from meteorological  
195 field simulations might constitute one of the most possible reasons for the RH bias (Bei et al.,  
196 2017). Figure 4 presents the pattern comparison of the average simulated RH and the NCEP  
197 reanalysis during the episode. The simulated RH distribution is generally consistent with that  
198 from the reanalysis, e.g., dry air in West China and fairly humid air in South China. However,



199 the air over NCP in the simulation is more humid than the analysis, and the average simulated  
200 RH is 70.6%, about 20% higher than the reanalyzed RH, which might be caused by the  
201 temperature decrease due to the ARF considered in the simulation.

### 202 3.3 Sensitivity studies

203 The ALW not only enlarges the particle size to increase the aerosol optical depth (AOD),  
204 likely enhancing the ARF to facilitate the PM<sub>2.5</sub> accumulation or to alter photolysis rates to  
205 affect the AOC, but also influences the SA formation serving as a medium for multiphase  
206 reactions. Therefore, sensitivity studies are used to quantitatively evaluate the effect of the  
207 ALW on the PM<sub>2.5</sub> concentration during the haze pollution episode.

208 The FSA method was used to evaluate the contribution of the ALW to near-surface  
209 [PM<sub>2.5</sub>] by differentiating two model simulations with and without the ALW effect. Besides  
210 the base case with all the ALW effect (hereafter referred as to  $f_{base}$ ), additional four  
211 sensitivity simulations were performed, in which the ALW effect on the ARF, photolysis,  
212 multiphase reactions, and the total were excluded, respectively (hereafter referred as to  
213  $f_{alw-rad0}$ ,  $f_{alw-j0}$ ,  $f_{alw-het0}$ , and  $f_{alw-tot0}$ , respectively)

#### 214 3.3.1 ALW effect on the ARF

215 The ALW, caused by the aerosol hygroscopic growth, augments the particle size to  
216 increase AOD, potentially enhancing the ARF and aggravating the haze pollution. Figure 5  
217 shows the distribution of the average AOD contribution due to the ALW during the haze  
218 episode, evaluated by differentiating  $f_{base}$  and  $f_{alw-rad0}$ . Apparently, the ALW  
219 substantially increases the AOD in NCP, with the contribution ranging from 30% to more  
220 than 50%, indicating that ALW is an important contributor of the AOD. Substantial increase  
221 of the AOD due to the ALW is anticipated to attenuate the incoming solar radiation,  
222 decreasing the surface temperature and suppressing the PBL development, therefore,  
223 deteriorating the haze pollution, as proposed by recent studies (Tie et al., 2017; Liu et al.,



224 2018).

225 Figure 6 presents the distribution of the average near-surface  $\text{PM}_{2.5}$  contribution of the  
226 ALW effect on the ARF (hereafter referred as to ALW-ARF) during the haze episode.  
227 Interestingly, the ALW-ARF does not increase the near-surface  $[\text{PM}_{2.5}]$  consistently in NCP,  
228 as expected. The ALW-ARF enhances the near-surface  $[\text{PM}_{2.5}]$  most strikingly in the south of  
229 Hebei, with a contribution of more than  $15 \mu\text{g m}^{-3}$  (less than 7%). However, in some areas,  
230 such as the east of Shandong, the near-surface  $\text{PM}_{2.5}$  contribution of the ALW-ARF is  
231 negative, or the ALW-ARF decreases  $[\text{PM}_{2.5}]$ . On average, the ALW-ARF increases  
232 near-surface  $[\text{PM}_{2.5}]$  in NCP during the episode by about  $1.1 \mu\text{g m}^{-3}$ , so cannot constitute an  
233 important factor for the heavy haze formation.

234 It is worth noting that enlarged particles due to the ALW not only increase the AOD to  
235 enhance aerosol backward scattering, but also cause the aerosol spectrum to successively  
236 shift toward larger sizes. Based on the Mie scattering theory, when the particle size is similar  
237 to the wavelength of incoming solar radiation, the radiation is favored to be scattered in the  
238 forward directions. In order to further verify the ALW effect on solar radiation and  
239 near-surface  $[\text{PM}_{2.5}]$ , an ensemble method is employed similar to that reported in Wu et al.  
240 (2018a). The daytime near-surface  $[\text{PM}_{2.5}]$  in NCP during the episode in  $f_{base}$  are first  
241 subdivided into 30 bins with the interval of  $20 \mu\text{g m}^{-3}$ . The AOD at 550 nm, aerosol effective  
242 radius ( $\text{Reff}$ ), downward shortwave radiation at the surface (SWDOWN), surface temperature  
243 (TSFC), PBLH, and near-surface  $[\text{PM}_{2.5}]$  in  $f_{base}$  and  $f_{alw-rad0}$  in the same grid cell are  
244 assembled as the bin  $[\text{PM}_{2.5}]$ , respectively, and an average of these variables in each bin are  
245 calculated. Figure 7 shows the variation of AOD and  $\text{Reff}$  in  $f_{base}$  and  $f_{alw-rad0}$  as a  
246 function of bin  $[\text{PM}_{2.5}]$ . The ALW not only significantly enhances the AOD, with an average  
247 contribution of 46% in NCP during the episode, but also increases the  $\text{Reff}$  considerably  
248 (Figures 7a and 7b). The  $\text{Reff}$  enhancement due to the ALW is the most striking with



249 near-surface  $[PM_{2.5}]$  between 40 and  $160 \mu\text{g m}^{-3}$ , exceeding 60%. On average, the ALW  
250 increases the  $Reff$  from  $0.31 \mu\text{m}$  to  $0.48 \mu\text{m}$ , close to the peak band of solar radiation.  
251 Therefore, the ALW increases the AOD to scatter more incoming solar radiation, decreasing  
252 the SWDOWN, but augments particle sizes to favor the forward scattering, increasing the  
253 SWDOWN. Generally, the decrease of the SWDOWN caused by the ALW is not significant,  
254 less than 1% with near-surface  $[PM_{2.5}]$  less than  $200 \mu\text{g m}^{-3}$  and ranging from 2% to 3% with  
255  $[PM_{2.5}]$  exceeding  $240 \mu\text{g m}^{-3}$  (Figure 8a). Correspondingly, the ALW-ARF effect on the  
256 daytime TSFC is also marginal and the TSFC is decreased by less than  $0.2^\circ\text{C}$  (Figure 8b).  
257 Furthermore, the ALW-ARF generally increases the daytime PBLH with near-surface  $[PM_{2.5}]$   
258 less than  $140 \mu\text{g m}^{-3}$ , but are opposite with  $[PM_{2.5}]$  exceeding  $140 \mu\text{g m}^{-3}$  (Figure 8c). Hence,  
259 the contribution of the ALW-ARF to near-surface  $[PM_{2.5}]$  is highly uncertain (Figure 8d),  
260 depending on the relative importance of the ALW induced enhancement of aerosol backward  
261 and forward scattering.

### 262 3.3.2 ALW effect on the photochemistry

263 In addition to the ARF, the ALW also exerts an impact on the photochemistry by altering  
264 the aerosol backward and forward scattering to affect the photolysis, further influencing the  
265 ozone ( $O_3$ ) and SA formation. Previous studies have shown that the ALW modifies the  
266 vertical profile of photolysis rate of  $NO_2$  ( $J_{NO_2}$ ), inhibiting it at the ground level and  
267 accelerating it in the upper PBL (Tao et al., 2014; Dickerson et al., 1997). The combination  
268 reaction between the ground state oxygen atom ( $O(^3P)$ ), produced from  $NO_2$  photolysis, and  
269 oxygen molecules ( $O_2$ ) forms  $O_3$ , representing the only important source of  $O_3$  in the  
270 troposphere:



273 Thus, the variation of  $J_{NO_2}$  considerably affects the  $O_3$  formation in the troposphere,



274 changing the AOC and further the SA formation.

275 Figures 9a and 9b present the distribution of the percentage variation of average daytime  
276  $J_{NO_2}$  due to the ALW during the haze episode at the 1<sup>st</sup> and 5<sup>th</sup> model layer, respectively. At  
277 the 1<sup>st</sup> model layer, except in the north of Jiangsu, the ALW generally decreases  $J_{NO_2}$   
278 slightly in NCP. However, at 5<sup>th</sup> model layer, the region with enhanced  $J_{NO_2}$  caused by the  
279 ALW is obviously increased compared to that at 1<sup>st</sup> model layer. Apparently, the ALW  
280 induced enlargement of particle sizes increases the AOD and enhances the aerosol backward  
281 scattering to reduce the solar radiation reaching the ground level, decreasing the photolysis  
282 rate, but the enhanced forward scattering still potentially accelerates the photolysis, such as in  
283 the north of Jiangsu. In addition, the enhanced aerosol backward scattering also increases the  
284 photolysis rate in the upper and above PBL, which is consistent with previous studies (Tao et  
285 al., 2014; Dickerson et al., 1997). The variation of average daytime  $O_3$  concentrations is not  
286 consistent with that of  $J_{NO_2}$  at the 1<sup>st</sup> model layer (Figure 9c). For example, although the  
287  $J_{NO_2}$  is decreased in Hebei and Shandong, the  $O_3$  concentration is still enhanced by the ALW  
288 in some areas of the two provinces. One of the possible reasons is the vertical transport of  $O_3$   
289 from the upper layers where the  $O_3$  is plausibly enhanced due to the increased photolysis rate  
290 (Figure 9b). At the 5<sup>th</sup> model layer, the area with enhanced  $O_3$  concentrations is much larger  
291 than that at 1<sup>st</sup> model layer, which is in agreement with the variation of the  $J_{NO_2}$  (Figure 9d).  
292 On average, the ALW decreases near-surface (1<sup>st</sup> model layer) daytime  $O_3$  concentrations by  
293 about  $0.2 \mu\text{g m}^{-3}$  (or 0.45%), playing a minor role in  $O_3$  formation.

294 Figure 10 shows the distribution of the average near-surface  $PM_{2.5}$  contribution of the  
295 ALW effect on the photolysis frequencies (hereafter referred as to ALW-J) during the haze  
296 episode. Except in some areas in Shandong and Anhui, the ALW-J slightly decreases  
297 near-surface  $[PM_{2.5}]$  in NCP, with an average reduction of about  $0.87 \mu\text{g m}^{-3}$  (or 0.64%).  
298 Therefore, the ALW-J does not play an important role in mitigating the haze pollution.



### 299 3.3.3 ALW effect on heterogeneous reactions

300 The ALW provides an excellent substrate for heterogeneous reactions in the atmosphere,  
301 which have been proposed to play a key role in the SA formation during haze days (Li et al.,  
302 2017; Xing et al., 2018).

303 Figure 11 presents the distribution of contributions of the ALW on heterogeneous  
304 reactions (hereafter referred to ALW-HET) to near-surface sulfate, nitrate, and ammonium  
305 concentrations averaged during the haze episode. A parameterization of sulfate heterogeneous  
306 formation involving ALW has been developed and implemented into the WRF-CHEM model,  
307 which has successfully reproduced the observed rapid sulfate formation during haze days (Li  
308 et al., 2017). The sulfate heterogeneous formation from SO<sub>2</sub> is parameterized as a first order  
309 irreversible uptake by ALW surfaces, with a reactive uptake coefficient of  $0.5 \times 10^{-4}$  assuming  
310 that there is enough alkalinity to maintain the high iron-catalyzed reaction rate. The  
311 contribution of the ALW-HET to the sulfate formation is substantial in NCP, exceeding 5 μg  
312 m<sup>-3</sup> (or 50%) in NCP (Figures 11a and 11b). The ALW-HET contributes about 71.3% of the  
313 sulfate in NCP during the episode, indicating that the heterogeneous formation involving the  
314 ALW is the dominant sulfate source during haze days.

315 The heterogeneous hydrolysis of N<sub>2</sub>O<sub>5</sub> on the surface of deliquescent aerosols leads to  
316 the HNO<sub>3</sub> formation, which is the key contributor to the nitrate aerosol loading (Riemer et al.,  
317 2003; Pathak et al., 2011; Chang et al., 2016). In this study, the parameterization of the  
318 heterogeneous hydrolysis of N<sub>2</sub>O<sub>5</sub>, proposed by Riemer et al. (2003), has been included in the  
319 WRF-CHEM model for considering the effect of ALW-HET on the nitrate formation. The  
320 N<sub>2</sub>O<sub>5</sub> uptake coefficient on wet aerosol surfaces ranges from 0.002 to 0.02, depending on the  
321 sulfate and nitrate aerosol mass. The ALW-HET generally increases the near-surface nitrate  
322 mass concentration by 2 to 8 μg m<sup>-3</sup> in NCP, with an average contribution of 2.8 μg m<sup>-3</sup> (or  
323 10%) (Figures 11c and 11d). It is worth noting that the ALW-HET does not consistently



324 increase the nitrate formation and the nitrate concentration is considerably decreased in some  
325 areas in east China. One of the possible reasons is that the ALW-HET substantially enhances  
326 the sulfate formation and the increased sulfate competes with nitrate for ammonia (NH<sub>3</sub>),  
327 suppressing the nitrate formation. Figure 12 shows the distribution of the NH<sub>3</sub> emission rate  
328 in December. High NH<sub>3</sub> emissions are concentrated in NCP, Central China, Sichuan basin,  
329 and Northeast China, where the nitrate concentration is generally increased by the ALW-HET.

330 Ammonium serves as the main alkali in the atmosphere to neutralize acidic aerosols  
331 such as sulfate and nitrate, so its formation is not only dependent on its precursor (NH<sub>3</sub>), but  
332 is also influenced by acid aerosols. The ALW-HET enhances the near-surface ammonium  
333 mass concentration most strikingly in NCP with high NH<sub>3</sub> emissions and increased sulfate  
334 and nitrate aerosols. The contribution of the ALW-HET to the ammonium concentration  
335 varies from 2 to more than 10 μg m<sup>-3</sup>, with an average of 4.2 μg m<sup>-3</sup> (or 25.6%), showing that  
336 the heterogeneous formation constitutes an important ammonium source (Figures 11e and  
337 11f).

338 Heterogeneous reactions are also an important pathway for the SOA formation (Fu et al.,  
339 2008; Li et al., 2013). Laboratory and field studies have indicated that glyoxal and  
340 methylglyoxal play an important role in SOA formation via aerosol uptake or cloud  
341 processing (Liggio et al., 2005; Volkamer et al., 2007; Li et al., 2011). In this study, the  
342 heterogeneous reaction of SOA formation from glyoxal and methylglyoxal is parameterized  
343 as a first-order irreversible uptake by aerosol particles, with a reaction uptake coefficient of  
344  $3.7 \times 10^{-3}$  (Liggio et al., 2005; Zhao et al., 2006; Volkamer et al., 2007; Li et al., 2011).  
345 During the haze episode, the average near-surface SOA contribution of the ALW-HET is 7.4  
346 μg m<sup>-3</sup> (or 48%) in NCP, ranging from 3 to over 15 μg m<sup>-3</sup> (or 30 to over 50%) in NCP,  
347 showing that heterogeneous reactions of glyoxal and methylglyoxal on wet aerosol surfaces  
348 play a critical role in SOA formation (Figure 13). Xing et al. (2018) have demonstrated that,



349 in Beijing-Tianjin-Hebei, the near-surface SOA contribution from glyoxal and methylglyoxal  
350 is around 30% during a haze episode in January 2014, much less than that (48%) in the study.  
351 The possible reason is that the RH in the episode is higher than that in Xing et al. (2018),  
352 causing more SOA formation from glyoxal and methylglyoxal.

353 High SA contribution to the haze pollution has been observed in China (e.g., Huang et  
354 al., 2014), so the ALW-HET substantially enhances the SA formation, constituting an  
355 important factor for heavy haze formation. Figure 14 shows the contribution of the  
356 ALW-HET to average near-surface  $[PM_{2.5}]$  during the study episode. The ALW-HET  
357 enhances near-surface  $[PM_{2.5}]$  by more than  $40 \mu\text{g m}^{-3}$  in the central part of NCP, and on  
358 average, the  $PM_{2.5}$  contribution of the ALW-HET is  $21.7 \mu\text{g m}^{-3}$  (or 15.9%), less than the total  
359 enhancement of  $25.1 \mu\text{g m}^{-3}$  (or 18.4%) from sulfate, nitrate, ammonium, and SOA. The  
360 inconsistency indicates that the ALW-HET induced SA enhancement causes a decrease in  
361 primary aerosols. Figure 15a and 15b show the percentage decrease of black carbon (BC) and  
362 primary organic aerosols (POA) as a function of bin  $[PM_{2.5}]$ , respectively. Interestingly, the  
363 average BC and POA concentrations are decreased by 5.1% and 5.2% due to the ALW-HET,  
364 respectively. The ALW-HET induced SA enhancement augments the particle size and should  
365 increase the AOD. However, on the contrary, the ALW-HET decreases the AOD, although  
366 considerably increases the  $Reff$  (Figures 16a and 16b). The reason is that the enhanced SA  
367 enlarges particle sizes, facilitating the coagulation to decrease the aerosol number  
368 concentration and surface area, as shown in Figures 16c and 16d. Hence, the decreased AOD  
369 and increased  $Reff$  due to the ALW-HET enhance the SWDOWN and TSFC, further  
370 increasing the PBLH and decreasing near-surface primary aerosols, as shown in Figure 17.

### 371 3.3.4 ALW total effect

372 Above discussions have shown that the ALW influences near-surface  $[PM_{2.5}]$  through  
373 complicated physical and chemical processes, which interact with each other. Figure 18



374 shows the near-surface  $\text{PM}_{2.5}$  contribution of the total ALW effect (hereafter referred as to  
375 ALW-TOT) during the haze episode, evaluated by differentiating  $f_{base}$  and  $f_{alw-tot0}$ . The  
376 ALW-TOT plays an important role in the  $\text{PM}_{2.5}$  formation during the wintertime haze  
377 pollution in NCP, with an average contribution of  $23.8 \mu\text{g m}^{-3}$  (or 17.5%), ranging from 5 to  
378 over  $40 \mu\text{g m}^{-3}$ . About 78% of the enhanced near-surface  $[\text{PM}_{2.5}]$  due to the ALW-TOT is  
379 contributed by secondary inorganic aerosols, in which the contributions from sulfate, nitrate,  
380 and ammonium are 45%, 14% and 19%, respectively, and around 32% is contributed by SOA.  
381 Therefore, about 10% of near-surface  $[\text{PM}_{2.5}]$  enhancement from SA is counterbalanced by  
382 the decrease in the primary aerosols. Therefore, the ALW induced enhancement of  
383 near-surface  $[\text{PM}_{2.5}]$  is overwhelmingly determined by the ALW-HET, and the ALW-ARF  
384 and ALW-J are subject to decreasing  $[\text{PM}_{2.5}]$ .

385 Figure 19 shows the variation of near-surface  $[\text{PM}_{2.5}]$  caused by the ALW-TOT,  
386 ALW-HET, ALW-ARF, and ALW-J, respectively, as a function of bin near-surface RH in  
387 NCP during the haze episode to further assess the ALW effect. The hourly near-surface RH in  
388  $f_{base}$  is first divided into 28 bins, ranging from 30% to 100%, with interval of 2.5%. The  
389  $\text{PM}_{2.5}$  contribution from the four sensitivity simulations is assembled in the same grid cell as  
390 the bin RH, and an average of  $\text{PM}_{2.5}$  contribution in each bin is calculated. The ALW does not  
391 continuously increase near-surface  $[\text{PM}_{2.5}]$  with the RH. When the RH is less than 80%, the  
392 near-surface  $\text{PM}_{2.5}$  contribution of the ALW-TOT generally increases rapidly with the RH.  
393 However, when the RH exceeds 80%, the contribution commences to decrease and fluctuates  
394 between  $20$  and  $30 \mu\text{g m}^{-3}$ , showing the effect of high occurrence frequencies of precipitation.  
395 In addition, the ALW-HET dominates the  $\text{PM}_{2.5}$  contribution, particularly with RH less than  
396 50%. The ALW-RAD generally decreases  $[\text{PM}_{2.5}]$  slightly with the RH less than 52.5% and  
397 vice versa with the RH more than 52.5%. The  $\text{PM}_{2.5}$  contribution of the ALW-J is negative  
398 and less than  $1.5 \mu\text{g m}^{-3}$ , except when the RH is between 92.5% and 97.5%.



399

**400 4 Conclusions and summaries**

401 The good relationships between near-surface  $[PM_{2.5}]$  concentration and RH during the  
402 wintertime of 2015 in NCP indicate the possibility that high RH plays an important role in the  
403  $PM_{2.5}$  formation during the haze pollution. A severe haze pollution episode from 05  
404 December 2015 to 04 January 2016 is simulated using the WRF-CHEM model to investigate  
405 the impact of ALW caused by the accumulated moisture on near surface  $[PM_{2.5}]$  in NCP. The  
406 air over NCP during the haze episode is humid, with an average simulated RH of about 71%.  
407 In general, the WRF-CHEM model reproduces reasonably well the temporal variations of RH  
408 compared to observations at three sites in NCP, although the model biases still exist due to  
409 the uncertainties in simulated meteorological fields.

410 The FSA method is used to evaluate the contribution of the ALW effect on ARF,  
411 photochemistry and heterogeneous reactions to the wintertime  $PM_{2.5}$  concentration in NCP.  
412 Model results show that the ALW substantially increases the daytime AOD with an average  
413 contribution of 46% in NCP during the episode, enhancing the aerosol backward scattering,  
414 and also augments the  $Reff$  from 0.31  $\mu m$  to 0.48  $\mu m$ , approaching the peak band of solar  
415 radiation, favoring the aerosol forward scattering. The ALW does not significantly attenuate  
416 the incoming solar radiation at the ground surface to enhance the ARF, and the average  
417 near-surface  $PM_{2.5}$  contribution of the ALW-ARF is about 1.1  $\mu g m^{-3}$  in NCP during the  
418 episode. Therefore, the ALW-ARF is not an important factor for heavy haze formation and its  
419 contribution relies on the relative importance of the ALW induced enhancement of aerosol  
420 backward and forward scattering. The ALW generally decreases the photolysis rate at the  
421 surface level due to enhanced backward aerosol scattering, but the favored forward scattering  
422 still possibly accelerates the photolysis. Additionally, the ALW increases the photolysis rate  
423 in the upper and above PBL. On average, the ALW decreases near-surface daytime  $O_3$



424 concentrations by  $0.20 \mu\text{g m}^{-3}$  and  $[\text{PM}_{2.5}]$  by  $0.87 \mu\text{g m}^{-3}$ , playing a minor role in mitigating  
425 the haze pollution.

426 The ALW substantially enhances the SA formation by serving as an important medium  
427 for liquid-phase and heterogeneous reactions. The ALW contribution to near-surface sulfate,  
428 nitrate, ammonium, and SOA concentrations is 71%, 10%, 26%, and 48% in NCP during the  
429 episode, respectively. However, the enhanced SA due to the ALW-HET enlarges particle sizes  
430 to facilitate the coagulation, decreasing the aerosol number concentration and surface area  
431 and further AOD. Therefore, the decreased AOD and increased  $\text{Reff}$  enhance the incoming  
432 solar radiation reaching the ground surface, further increasing the surface temperature and  
433 PBLH and decreasing near-surface primary aerosols. The ALW-HET contributes 15.9% of  
434 near-surface  $[\text{PM}_{2.5}]$ , less than the total SA enhancement of 18.4%, and the rest is  
435 counterbalanced by the decrease in primary aerosols.

436 The near-surface  $\text{PM}_{2.5}$  contribution of the ALW total effect is 17.5% in NCP, indicating  
437 that ALW plays an important role in the  $\text{PM}_{2.5}$  formation during the wintertime haze pollution.  
438 Moreover, the ALW-HET overwhelmingly dominates the  $\text{PM}_{2.5}$  enhancement due to the ALW.  
439 The ALW does not consistently enhance near-surface  $[\text{PM}_{2.5}]$  with increasing RH. When the  
440 RH exceeds 80%, the contribution of the ALW commences to decrease caused by the high  
441 occurrence frequencies of precipitation.

442 Although the model performs reasonably well in simulating air pollutants, aerosol  
443 species and optical properties, and RH during the episode in NCP, the uncertainties from  
444 meteorological fields and emission inventory still exist, leading to model biases. In addition,  
445 simulation period of one month might not be sufficient to provide a comprehensive view of  
446 the ALW effect on the  $\text{PM}_{2.5}$  formation. More wintertime case studies will need to be  
447 performed in the future to further investigate the ALW effect.

448



449

450 *Author contribution.* Guohui Li, as the contact author, provided the ideas and financial  
451 support, developed the model code, verified the conclusions, and revised the paper. Jiarui Wu  
452 conducted a research, designed the experiments, carried the methodology out, performed the  
453 simulation, processed the data, prepared the data visualization, and prepared the manuscript  
454 with contributions from all authors. Naifang Bei provided the treatment of meteorological  
455 data, analyzed the study data, validated the model performance, and reviewed the manuscript.  
456 Bo Hu provided the observation data used in the study, synthesized the observation, and  
457 reviewed the paper. Suixin Liu, Meng Zhou, Qiyuan Wang, Zirui Liu, and Yichen Wang  
458 provided the data and the primary data process, and reviewed the manuscript. Xia Li, Lang  
459 Liu, and Tian Feng analyzed the initial simulation data, visualized the model results and  
460 reviewed the paper. Junji Cao, Xuexi Tie, Jun Wang provided critical reviews pre-publication  
461 stage. Luisa T. Molina provided a critical preview and financial support, and revised the  
462 manuscript.

463

464

465 *Acknowledgements.* This work is financially supported by the National Key R&D Plan  
466 (Quantitative Relationship and Regulation Principle between Regional Oxidation Capacity of  
467 Atmospheric and Air Quality (2017YFC0210000)) and National Research Program for Key  
468 Issues in Air Pollution Control. Luisa Molina acknowledges support from US NSF Award  
469 1560494.

470

471

472

473

474

**475 Reference**

- 476** Ackerman, T., and Baker, M. B.: Shortwave radiative effects of unactivated aerosol-particles  
**477** in clouds, *J. Appl. Meteorol.*, 16, 63-69,  
**478** 10.1175/1520-0450(1977)016<0063:sreoua>2.0.co;2, 1977.
- 479** Ackerman, T. P.: Model of effect of aerosols on urban climates with particular applications to  
**480** Los-angeles basin, *J. Atmos. Sci.*, 34, 531-547,  
**481** 10.1175/1520-0469(1977)034<0531:amoteo>2.0.co;2, 1977.
- 482** Bei, N. F., Li, G. H., Huang, R. J., Cao, J. J., Meng, N., Feng, T., Liu, S. X., Zhang, T., Zhang,  
**483** Q., and Molina, L. T.: Typical synoptic situations and their impacts on the wintertime air  
**484** pollution in the Guanzhong basin, China, *Atmos. Chem. Phys.*, 16, 7373-7387,  
**485** 10.5194/acp-16-7373-2016, 2016a.
- 486** Bei, N. F., Xiao, B., Meng, N., and Feng, T.: Critical role of meteorological conditions in a  
**487** persistent haze episode in the Guanzhong basin, China, *Sci. Total Environ.*, 550,  
**488** 273-284, 10.1016/j.scitotenv.2015.12.159, 2016b.
- 489** Bei, N. F., Wu, J. R., Elser, M., Feng, T., Cao, J. J., El-Haddad, I., Li, X., Huang, R. J., Li, Z.  
**490** Q., Long, X., Xing, L., Zhao, S. Y., Tie, X. X., Prevot, A. S. H., and Li, G. H.: Impacts  
**491** of meteorological uncertainties on the haze formation in Beijing-Tianjin-Hebei (BTH)  
**492** during wintertime: a case study, *Atmos. Chem. Phys.*, 17, 14579-14591,  
**493** 10.5194/acp-17-14579-2017, 2017.
- 494** Blando, J. D., and Turpin, B. J.: Secondary organic aerosol formation in cloud and fog  
**495** droplets: a literature evaluation of plausibility, *Atmos. Environ.*, 34, 1623-1632,  
**496** 10.1016/s1352-2310(99)00392-1, 2000.
- 497** Carrico, C. M., Kus, P., Rood, M. J., Quinn, P. K., and Bates, T. S.: Mixtures of pollution,  
**498** dust, sea salt, and volcanic aerosol during ACE-Asia: Radiative properties as a function  
**499** of relative humidity, *J. Geophys. Res.-Atmos.*, 108, 18, 10.1029/2003jd003405, 2003.
- 500** Chan, C. K. and Yao, X.: Air pollution in mega cities in China, *Atmos. Environ.*, 42, 1-42,  
**501** 2008.
- 502** Chang, W. L., Brown, S. S., Stutz, J., Middlebrook, A. M., Bahreini, R., Wagner, N. L., Dube,  
**503** W. P., Pollack, I. B., Ryerson, T. B., and Riemer, N.: Evaluating N<sub>2</sub>O<sub>5</sub> heterogeneous  
**504** hydrolysis parameterizations for CalNex 2010, *J. Geophys. Res.-Atmos.*, 121,  
**505** 5051-5070, 10.1002/2015jd024737, 2016.
- 506** Chen, F. and Dudhia, J.: Coupling an advanced land surface-hydrology model with the Penn  
**507** State-NCAR MM5 modeling system. Part I: Model implementation and sensitivity, *Mon.*  
**508** *Weather Rev.*, 129(4), 569-585, 2001.
- 509** Cheng, Y., He, K. B., Du, Z. Y., Zheng, M., Duan, F. K., and Ma, Y. L.: Humidity plays an  
**510** important role in the PM<sub>2.5</sub> pollution in Beijing, *Environ. Pollut.*, 197, 68-75,  
**511** 10.1016/j.envpol.2014.11.028, 2015.
- 512** Cheng, Y. F., Wiedensohler, A., Eichler, H., Heintzenberg, J., Tesche, M., Ansmann, A.,  
**513** Wendisch, M., Su, H., Althausen, D., Herrmann, H., Gnauk, T., Brüggemann, E., Hu, M.,  
**514** and Zhang, Y. H.: Relative humidity dependence of aerosol optical properties and direct  
**515** radiative forcing in the surface boundary layer at Xinken in Pearl River Delta of China:  
**516** An observation based numerical study, *Atmos. Environ.*, 42, 6373-6397,  
**517** 10.1016/j.atmosenv.2008.04.009, 2008.



- 518 Chou, M.-D. and Suarez, M. J.: A solar radiation parameterization for atmospheric studies,  
519 NASA Tech. Rep. NASA/TM-1999-10460, 15, 38 pp., 1999.
- 520 Chou, M.-D. and Suarez, M. J.: A thermal infrared radiation parameterization for  
521 atmospheric studies, NASA/TM-2001-104606, 19, 55 pp., 2001.
- 522 Cocker, D. R., Clegg, S. L., Flagan, R. C., and Seinfeld, J. H.: The effect of water on  
523 gas-particle partitioning of secondary organic aerosol. Part I: alpha-pinene/ozone system,  
524 Atmos. Environ., 35, 6049-6072, 10.1016/s1352-2310(01)00404-6, 2001a.
- 525 Cocker, D. R., Flagan, R. C., and Seinfeld, J. H.: State-of-the-art chamber facility for  
526 studying atmospheric aerosol chemistry, Environ. Sci. Technol., 35, 2594-2601,  
527 10.1021/es0019169, 2001b.
- 528 Cocker, D. R., Mader, B. T., Kalberer, M., Flagan, R. C., and Seinfeld, J. H.: The effect of  
529 water on gas-particle partitioning of secondary organic aerosol: II. m-xylene and  
530 1,3,5-trimethylbenzene photooxidation systems, Atmos. Environ., 35, 6073-6085,  
531 10.1016/s1352-2310(01)00405-8, 2001c.
- 532 Covert, D. S., Charlson, R. J., and Ahlquist, N. C.: A Study of the Relationship of Chemical  
533 Composition and Humidity to Light Scattering by Aerosols, J. Appl. Meteorol., 11,  
534 968-976, 1972.
- 535 Dickerson, R. R., Kondragunta, S., Stenchikov, G., Civerolo, K. L., Doddridge, B. G., and  
536 Holben, B. N.: The impact of aerosols on solar ultraviolet radiation and photochemical  
537 smog, Science, 278, 827-830, 10.1126/science.278.5339.827, 1997.
- 538 Ding, Y. H., Wu, P., Liu, Y. J., and Song, Y. F.: Environmental and Dynamic Conditions for  
539 the Occurrence of Persistent Haze Events in North China, Engineering, 3, 266-271,  
540 10.1016/j.eng.2017.01.009, 2017.
- 541 Flocas, H., Kelessis, A., Helmis, C., Petrakakis, M., Zoumakis, M., and Pappas, K.: Synoptic  
542 and local scale atmospheric circulation associated with air pollution episodes in an urban  
543 Mediterranean area, Theo. Appl. Climatol., 95, 265-277, 10.1007/s00704-008-0005-9,  
544 2009.
- 545 Fu, G. Q., Xu, W. Y., Yang, R. F., Li, J. B., and Zhao, C. S.: The distribution and trends of fog  
546 and haze in the North China Plain over the past 30 years, Atmos. Chem. Phys., 14,  
547 11949-11958, 10.5194/acp-14-11949-2014, 2014.
- 548 Fu, T. M., Jacob, D. J., Wittrock, F., Burrows, J. P., Vrekoussis, M., and Henze, D. K.: Global  
549 budgets of atmospheric glyoxal and methylglyoxal, and implications for formation of  
550 secondary organic aerosols, J. Geophys. Res.-Atmos., 113, 17, 10.1029/2007jd009505,  
551 2008.
- 552 Gabusi, V., Pisoni, E., and Volta, M.: Factor separation in air quality simulations, Ecol.  
553 Model., 218, 383-392, 10.1016/j.ecolmodel.2008.07.030, 2008.
- 554 Guenther, A., Karl, T., Harley, P., Wiedinmyer, C., Palmer, P. I., and Geron, C.: Estimates of  
555 global terrestrial isoprene emissions using MEGAN (Model of Emissions of Gases and  
556 Aerosols from Nature), Atmos. Chem. Phys., 6, 3181-3210,  
557 <https://doi.org/10.5194/acp-6-3181-2006>, 2006.
- 558 Guo, S., Hu, M., Zamora, M. L., Peng, J. F., Shang, D. J., Zheng, J., Du, Z. F., Wu, Z., Shao,  
559 M., Zeng, L. M., Molina, M. J., and Zhang, R. Y.: Elucidating severe urban haze  
560 formation in China, P. Natl. Acad. Sci. USA., 111, 17373-17378,



- 561 10.1073/pnas.1419604111, 2014.
- 562 Hallquist, M., Wenger, J. C., Baltensperger, U., Rudich, Y., Simpson, D., Claeys, M.,  
563 Dommen, J., Donahue, N. M., George, C., Goldstein, A. H., Hamilton, J. F., Herrmann,  
564 H., Hoffmann, T., Iinuma, Y., Jang, M., Jenkin, M. E., Jimenez, J. L., Kiendler-Scharr,  
565 A., Maenhaut, W., McFiggans, G., Mentel, T. F., Monod, A., Prevot, A. S. H., Seinfeld, J.  
566 H., Surratt, J. D., Szmigielski, R., and Wildt, J.: The formation, properties and impact of  
567 secondary organic aerosol: current and emerging issues, *Atmos. Chem. Phys.*, 9,  
568 5155-5236, 10.5194/acp-9-5155-2009, 2009.
- 569 Hastings, W. P., Koehler, C. A., Bailey, E. L., and De Haan, D. O.: Secondary organic aerosol  
570 formation by glyoxal hydration and oligomer formation: Humidity effects and  
571 equilibrium shifts during analysis, *Environ. Sci. Technol.*, 39, 8728-8735,  
572 10.1021/es050446l, 2005.
- 573 He, K. B., Yang, F. M., Ma, Y. L., Zhang, Q., Yao, X. H., Chan, C. K., Cadle, S., Chan, T.,  
574 and Mulawa, P.: The characteristics of PM<sub>2.5</sub> in Beijing, China, *Atmos. Environ.*, 35,  
575 4959-4970, 10.1016/s1352-2310(01)00301-6, 2001.
- 576 Healy, R. M., Temime, B., Kuprovskytė, K., and Wenger, J. C.: Effect of Relative Humidity  
577 on Gas/Particle Partitioning and Aerosol Mass Yield in the Photooxidation of p-Xylene,  
578 *Environ. Sci. Technol.*, 43, 1884-1889, 10.1021/es802404z, 2009.
- 579 Hong, S.-Y. and Lim, J.-O. J.: The WRF Single-Moment 6-Class Microphysics Scheme  
580 (WSM6), *Asia-Pacific J. Atmos. Sci.*, 42, 129-151, 2006.
- 581 Horowitz, L. W., Walters, S., Mauzerall, D. L., Emmons, L. K., Rasch, P. J., Granier, C., Tie,  
582 X. X., Lamarque, J. F., Schultz, M. G., Tyndall, G. S., Orlando, J. J., and Brasseur, G. P.:  
583 A global simulation of tropospheric ozone and related tracers: Description and  
584 evaluation of MOZART, version 2, *J. Geophys. Res.-Atmos.*, 108, 4784,  
585 <https://doi.org/10.1029/2002jd002853>, 2003.
- 586 Huang, R.-J., Zhang, Y., Bozzetti, C., Ho, K.-F., Cao, J.-J., Han, Y., Daellenbach, K. R.,  
587 Slowik, J. G., Platt, S. M., Canonaco, F., Zotter, P., Wolf, R., Pieber, S. M., Bruns, E. A.,  
588 Crippa, M., Ciarelli, G., Piazzalunga, A., Schwikowski, M., Abbaszade, G.,  
589 Schnelle-Kreis, J., Zimmermann, R., An, Z., Szidat, S., Baltensperger, U., El Haddad, I.,  
590 and Prévôt, A. S. H.: High secondary aerosol contribution to particulate pollution during  
591 haze events in China, *Nature*, 514, 218-222, doi: 10.1038/nature13774, 2014.
- 592 Im, J. S., Saxena, V. K., and Wenny, B. N.: An assessment of hygroscopic growth factors for  
593 aerosols in the surface boundary layer for computing direct radiative forcing, *J. Geophys.*  
594 *Res.-Atmos.*, 106, 20213-20224, 10.1029/2000jd000152, 2001.
- 595 Jacobson, M. Z.: Studying the effects of aerosols on vertical photolysis rate coefficient and  
596 temperature profiles over an urban airshed, *J. Geophys. Res.-Atmos.*, 103, 10593-10604,  
597 10.1029/98jd00287, 1998.
- 598 Jacobson, M. Z.: Analysis of aerosol interactions with numerical techniques for solving  
599 coagulation, nucleation, condensation, dissolution, and reversible chemistry among  
600 multiple size distributions, *J. Geophys. Res.-Atmos.*, 107, 23, 10.1029/2001jd002044,  
601 2002.
- 602 Janjic', Z. I.: Nonsingular Implementation of the Mellor -Yamada Level 2.5 Scheme in the  
603 NCEP Meso Model, *Ncep Office Note*, 436, 2002.
- 604 Jia, L., and Xu, Y. F.: Effects of Relative Humidity on Ozone and Secondary Organic Aerosol



- 605 Formation from the Photooxidation of Benzene and Ethylbenzene, *Aerosol Sci. Technol.*,  
606 48, 1-12, 10.1080/02786826.2013.847269, 2014.
- 607 Kamens, R. M., Zhang, H. F., Chen, E. H., Zhou, Y., Parikh, H. M., Wilson, R. L., Galloway,  
608 K. E., and Rosen, E. P.: Secondary organic aerosol formation from toluene in an  
609 atmospheric hydrocarbon mixture: Water and particle seed effects, *Atmos. Environ.*, 45,  
610 2324-2334, 10.1016/j.atmosenv.2010.11.007, 2011.
- 611 Kan, H. D., Chen, R. J., and Tong, S. L.: Ambient air pollution, climate change, and  
612 population health in China, *Environ. Int.*, 42, 10-19, 10.1016/j.envint.2011.03.003, 2012.
- 613 Koehler, C. A., Fillo, J. D., Ries, K. A., Sanchez, J. T., and De Haan, D. O.: Formation of  
614 secondary organic aerosol by reactive condensation of furandiones, aldehydes, and water  
615 vapor onto inorganic aerosol seed particles, *Environ. Sci. Technol.*, 38, 5064-5072,  
616 10.1021/es034672b, 2004.
- 617 Kurokawa, J., Ohara, T., Morikawa, T., Hanayama, S., Janssens- Maenhout, G., Fukui, T.,  
618 Kawashima, K., and Akimoto, H.: Emissions of air pollutants and greenhouse gases over  
619 Asian regions during 2000–2008: Regional Emission inventory in Asia (REAS) version  
620 2, *Atmos. Chem. Phys.*, 13, 11019–11058, <https://doi.org/10.5194/acp-13-11019-2013>,  
621 2013.
- 622 Li, G., Lei, W., Zavala, M., Volkamer, R., Dusanter, S., Stevens, P., and Molina, L. T.:  
623 Impacts of HONO sources on the photochemistry in Mexico City during the  
624 MCMA-2006/MILAGO Campaign, *Atmos. Chem. Phys.*, 10, 6551-6567,  
625 10.5194/acp-10-6551-2010, 2010.
- 626 Li, G., Bei, N., Tie, X., and Molina, L. T.: Aerosol effects on the photochemistry in Mexico  
627 City during MCMA-2006/MILAGRO campaign, *Atmos. Chem. Phys.*, 11, 5169-5182,  
628 10.5194/acp-11-5169-2011, 2011a.
- 629 Li, G., Zavala, M., Lei, W., Tsimpidi, A. P., Karydis, V. A., Pandis, S. N., agaratna, M. R., and  
630 Molina, L. T.: Simulations of organic aerosol concentrations in Mexico City using the  
631 WRF-CHEM model during the MCMA-2006/MILAGRO campaign, *Atmos. Chem.*  
632 *Phys.*, 11, 3789-3809, 10.5194/acp-11-3789-2011, 2011b.
- 633 Li, G., Lei, W., Bei, N., and Molina, L. T.: Contribution of garbage burning to chloride and  
634 PM<sub>2.5</sub> in Mexico City, *Atmos. Chem. Phys.*, 12, 8751-8761, 10.5194/acp-12-8751-2012,  
635 2012.
- 636 Li, G. H., Bei, N. F., Zavala, M., and Molina, L. T.: Ozone formation along the California  
637 Mexican border region during Cal-Mex 2010 field campaign, *Atmos. Environ.*, 88,  
638 370-389, 10.1016/j.atmosenv.2013.11.067, 2014.
- 639 Li, G., Bei, N., Cao, J., Huang, R., Wu, J., Feng, T., Wang, Y., Liu, S., Zhang, Q., Tie, X., and  
640 Molina, L. T.: A possible pathway for rapid growth of sulfate during haze days in China,  
641 *Atmos. Chem. Phys.*, 17, 3301–3316, <https://doi.org/10.5194/acp-17-3301-2017>, 2017a.
- 642 Li, N., Fu, T. M., Cao, J. J., Lee, S. C., Huang, X. F., He, L. Y., Ho, K. F., Fu, J. S., and Lam,  
643 Y. F.: Sources of secondary organic aerosols in the Pearl River Delta region in fall:  
644 Contributions from the aqueous reactive uptake of dicarbonyls, *Atmos. Environ.*, 76,  
645 200-207, 10.1016/j.atmosenv.2012.12.005, 2013.
- 646 Liggio, J., Li, S. M., and McLaren, R.: Reactive uptake of glyoxal by particulate matter, *J.*  
647 *Geophys. Res.-Atmos.*, 110, doi: 10.1029/2004jd005113, 2005.



- 648 Liu, Q., Jia, X. C., Quan, J. N., Li, J. Y., Li, X., Wu, Y. X., Chen, D., Wang, Z. F., and Liu, Y.  
649 G.: New positive feedback mechanism between boundary layer meteorology and  
650 secondary aerosol formation during severe haze events, *Sci. Rep.*, 8, 8,  
651 10.1038/s41598-018-24366-3, 2018.
- 652 Nguyen, T. B., Roach, P. J., Laskin, J., Laskin, A., and Nizkorodov, S. A.: Effect of humidity  
653 on the composition of isoprene photooxidation secondary organic aerosol, *Atmos. Chem.*  
654 *Phys.*, 11, 6931-6944, 10.5194/acp-11-6931-2011, 2011.
- 655 Parrish, D. D. and Zhu, T.: Clean Air for Megacities, *Science*, 326, 674–675,  
656 <https://doi.org/10.1126/science.1176064>, 2009.
- 657 Pathak, R. K., Wang, T., and Wu, W. S.: Nighttime enhancement of PM<sub>2.5</sub> nitrate in  
658 ammonia-poor atmospheric conditions in Beijing and Shanghai: Plausible contributions  
659 of heterogeneous hydrolysis of N<sub>2</sub>O<sub>5</sub> and HNO<sub>3</sub> partitioning, *Atmos. Environ.*, 45,  
660 1183-1191, 10.1016/j.atmosenv.2010.09.003, 2011.
- 661 Penner, J. E., Hegg, D., and Leaitch, R.: Unraveling the role of aerosols in climate change,  
662 *Environ. Sci. Technol.*, 35, 332A-340A, 10.1021/es0124414, 2001.
- 663 Poulain, L., Wu, Z., Petters, M. D., Wex, H., Hallbauer, E., Wehner, B., Massling, A.,  
664 Kreiden- weis, S. M., and Stratmann, F.: Towards closing the gap between hygroscopic  
665 growth and CCN activation for secondary organic aerosols - Part 3: Influence of the  
666 chemical composition on the hygroscopic properties and volatile fractions of aerosols,  
667 *Atmos. Chem. Phys.*, 10, 3775–3785, doi:10.5194/acp-10-3775-2010, 2010.
- 668 Pilinis, C., Seinfeld, J. H., and Grosjean, D.: Water content of atmospheric aerosols, *Atmos.*  
669 *Environ.*, 23, 1601–1606, 1989.
- 670 Quan, J. N., Gao, Y., Zhang, Q., Tie, X. X., Cao, J. J., Han, S. Q., Meng, J. W., Chen, P. F.,  
671 and Zhao, D. L.: Evolution of planetary boundary layer under different weather  
672 conditions, and its impact on aerosol concentrations, *Particuology*, 11, 34-40,  
673 10.1016/j.partic.2012.04.005, 2013.
- 674 Randles, C. A., Russell, L. M., and Ramaswamy, V.: Hygroscopic and optical properties of  
675 organic sea salt aerosol and consequences for climate forcing, *Geophys. Res. Lett.*, 31, 4,  
676 10.1029/2004gl020628, 2004.
- 677 Riemer, N., Vogel, H., Vogel, B., Schell, B., Ackermann, I., Kessler, C., and Hass, H.: Impact  
678 of the heterogeneous hydrolysis of N<sub>2</sub>O<sub>5</sub> on chemistry and nitrate aerosol formation in  
679 the lower troposphere under photochemical conditions, *J. Geophys. Res.-Atmos.*, 108, 21,  
680 10.1029/2002jd002436, 2003.
- 681 Seinfeld, J. H., Erdakos, G. B., Asher, W. E., and Pankow, J. F.: Modeling the formation of  
682 secondary organic aerosol (SOA). 2. The predicted effects of relative humidity on  
683 aerosol formation in the alpha-pinene-, beta-pinene-, sabinene-, Delta(3)-Carene-, and  
684 cyclohexene-ozone systems, *Environ. Sci. Technol.*, 35, 1806-1817, 10.1021/es001765+,  
685 2001.
- 686 Seinfeld, J. H. and Pandis, S. N.: *Atmospheric Chemistry and Physics: From Air Pollution to*  
687 *Climate Change*, John Wiley & Sons, USA, 1986.
- 688 Sun, Y., Wang, Z., Fu, P., Jiang, Q., Yang, T., Li, J., and Ge, X.: The impact of relative  
689 humidity on aerosol composition and evolution processes during wintertime in Beijing,  
690 China, *Atmos. Environ.*, 77, 927-934, 10.1016/j.atmosenv.2013.06.019, 2013.



- 691 Stein, U., and Alpert, P.: Factor separation in numerical simulations, *Journal of the*  
692 *Atmospheric Science*, 50, 2107-2115, 10.1175/1520-0469(1993)  
693 050<2107:fsins>2.0.co;2, 1993.
- 694 Tao, J. C., Zhao, C. S., Ma, N., and Liu, P. F.: The impact of aerosol hygroscopic growth on  
695 the single-scattering albedo and its application on the NO<sub>2</sub> photolysis rate coefficient,  
696 *Atmos. Chem. Phys.*, 14, 12055-12067, 10.5194/acp-14-12055-2014, 2014.
- 697 Tie, X. X., Huang, R. J., Cao, J. J., Zhang, Q., Cheng, Y. F., Su, H., Chang, D., Poschl, U.,  
698 Hoffmann, T., Dusek, U., Li, G. H., Worsnop, D. R., and O'Dowd, C. D.: Severe  
699 Pollution in China Amplified by Atmospheric Moisture, *Sci. Rep.*, 7, 8,  
700 10.1038/s41598-017-15909-1, 2017.
- 701 Volkamer, R., Martini, F. S., Molina, L. T., Salcedo, D., Jimenez, J. L., and Molina, M. J.: A  
702 missing sink for gas-phase glyoxal in Mexico City: Formation of secondary organic  
703 aerosol, *Geophys. Res. Lett.*, 34, 5, 10.1029/2007gl030752, 2007.
- 704 Wang, G., Zhang, R., Gomez, M. E., Yang, L., Zamora, M. L., Hu, M., Lin, Y., Peng, J., Guo,  
705 S., and Meng, J.: Persistent sulfate formation from London Fog to Chinese haze, *P. Natl.*  
706 *Acad. Sci. USA.*, 113, 13630–13635, 2016.
- 707 Wang, Y. S., Yao, L., Wang, L. L., Liu, Z. R., Ji, D. S., Tang, G. Q., Zhang, J. K., Sun, Y., Hu,  
708 B., and Xin, J. Y.: Mechanism for the formation of the January 2013 heavy haze  
709 pollution episode over central and eastern China, *Sci. China-Earth Sci.*, 57, 14-25,  
710 10.1007/s11430-013-4773-4, 2014.
- 711 Weinhold, B.: Ozone nation – EPA standard panned by the people, *Environ. Health. Persp.*,  
712 116, A302–A305, 2008.
- 713 Wu, J. R., Li, G. H., Cao, J. J., Bei, N. F., Wang, Y. C., Feng, T., Huang, R. J., Liu, S. X.,  
714 Zhang, Q., and Tie, X. X.: Contributions of trans-boundary transport to summertime air  
715 quality in Beijing, China, *Atmos. Chem. Phys.*, 17, 2035-2051,  
716 10.5194/acp-17-2035-2017, 2017.
- 717 Wu, P., Ding, Y. H., and Liu, Y. J.: Atmospheric circulation and dynamic mechanism for  
718 persistent haze events in the Beijing-Tianjin-Hebei region, *Adv. Atmos. Sci.*, 34,  
719 429-440, 10.1007/s00376-016-6158-z, 2017.
- 720 Wu, Z. J., Wang, Y., Tan, T. Y., Zhu, Y. S., Li, M. R., Shang, D. J., Wang, H. C., Lu, K. D.,  
721 Guo, S., Zeng, L. M., and Zhang, Y. H.: Aerosol Liquid Water Driven by Anthropogenic  
722 Inorganic Salts: Implying Its Key Role in Haze Formation over the North China Plain,  
723 *Environ. Sci. Technol. Lett.*, 5, 160-166, 10.1021/acs.estlett.8b00021, 2018.
- 724 Xing, L., Wu, J., Elser, M., Tong, S., Liu, S., Li, X., Liu, L., Cao, J., Zhou, J., El-Haddad, I.,  
725 Huang, R., Ge, M., Tie, X., Prévôt, A. S. H., and Li, G.: Wintertime secondary organic  
726 aerosol formation in Beijing-Tianjin-Hebei (BTH): Contributions of HONO sources and  
727 heterogeneous reactions, *Atmos. Chem. Phys. Discuss.*, 2018, 1-25,  
728 10.5194/acp-2018-770, 2018.
- 729 Xu, J. W., Martin, R. V., van Donkelaar, A., Kim, J., Choi, M., Zhang, Q., Geng, G., Liu, Y.,  
730 Ma, Z., Huang, L., Wang, Y., Chen, H., Che, H., Lin, P., and Lin, N.: Estimating  
731 ground-level PM<sub>2.5</sub> in eastern China using aerosol optical depth determined from the  
732 GOCI satellite instrument, *Atmos. Chem. Phys.*, 15, 13133-13144,  
733 10.5194/acp-15-13133-2015, 2015.



- 734 Zhang, L., Sun, J. Y., Shen, X. J., Zhang, Y. M., Che, H., Ma, Q. L., Zhang, Y. W., Zhang, X.  
735 Y., and Ogren, J. A.: Observations of relative humidity effects on aerosol light scattering  
736 in the Yangtze River Delta of China, *Atmos. Chem. Phys.*, 15, 8439-8454,  
737 [10.5194/acp-15-8439-2015](https://doi.org/10.5194/acp-15-8439-2015), 2015.
- 738 Zhang, Q., Streets, D. G., Carmichael, G. R., He, K. B., Huo, H., Kannari, A., Klimont, Z.,  
739 Park, I. S., Reddy, S., Fu, J. S., Chen, D., Duan, L., Lei, Y., Wang, L. T., and Yao, Z. L.:  
740 Asian emissions in 2006 for the NASA INTEX-B mission, *Atmos. Chem. Phys.*, 9,  
741 5131-5153, <https://doi.org/10.5194/acp-9-5131-2009>, 2009.
- 742 Zhang, R. H., Li, Q., and Zhang, R. N.: Meteorological conditions for the persistent severe  
743 fog and haze event over eastern China in January 2013, *Sci. China-Earth Sci.*, 57, 26-35,  
744 [10.1007/s11430-013-4774-3](https://doi.org/10.1007/s11430-013-4774-3), 2014.
- 745 Zhang, R., Jing, J., Tao, J., Hsu, S.-C., Wang, G., Cao, J., Lee, C. S. L., Zhu, L., Chen, Z.,  
746 Zhao, Y., and Shen, Z.: Chemical characterization and source apportionment of PM<sub>2.5</sub> in  
747 Beijing: seasonal perspective, *Atmos. Chem. Phys.*, 13, 7053-7074,  
748 <https://doi.org/10.5194/acp-13-7053-2013>, 2013.
- 749 Zhao, J., Levitt, N. P., Zhang, R. Y., and Chen, J. M.: Heterogeneous reactions of  
750 methylglyoxal in acidic media: implications for secondary organic aerosol formation,  
751 *Environ. Sci. Technol.*, 40, 7682-7687, 2006.
- 752 Zhou, Y., Zhang, H. F., Parikh, H. M., Chen, E. H., Rattanavaraha, W., Rosen, E. P., Wang, W.  
753 X., and Kamens, R. M.: Secondary organic aerosol formation from xylenes and mixtures  
754 of toluene and xylenes in an atmospheric urban hydrocarbon mixture: Water and particle  
755 seed effects (II), *Atmos. Environ.*, 45, 3882-3890, [10.1016/j.atmosenv.2010.12.048](https://doi.org/10.1016/j.atmosenv.2010.12.048),  
756 2011.  
757



758 Table 1 WRF-CHEM model configurations

759

Regions	East Asia
Simulation period	December 05, 2015 - January 04, 2016
Domain size	400 × 400
Domain center	35°N, 114°E
Horizontal resolution	12km × 12km
Vertical resolution	35 vertical levels with a stretched vertical grid with spacing ranging from 30 m near the surface, to 500 m at 2.5 km and 1 km above 14 km
Microphysics scheme	WSM 6-class graupel scheme (Hong and Lim, 2006)
Boundary layer scheme	MYJ TKE scheme (Janjić, 2002)
Surface layer scheme	MYJ surface scheme (Janjić, 2002)
Land-surface scheme	Unified Noah land-surface model (Chen and Dudhia, 2001)
Longwave radiation scheme	Goddard longwave scheme (Chou and Suarez, 2001)
Shortwave radiation scheme	Goddard shortwave scheme (Chou and Suarez, 1999)
Meteorological boundary and initial conditions	NCEP 1°×1° reanalysis data
Chemical initial and boundary conditions	MOZART 6-hour output (Horowitz et al., 2003)
Anthropogenic emission inventory	Developed by Zhang et al. (2009) and Li et al. (2017), 2012 base year, and SAPRC-99 chemical mechanism
Biogenic emission inventory	MEGAN model developed by Guenther et al. (2006)
Model spin-up time	28 hours

760

761

762

763

764



765

**Figure Captions**

- 766 Figure 1 (a) WRF-CHEM simulation domain with topography and (b) North China Plain. In  
767 (a), the blue circles represent centers of cities with ambient monitoring sites and the  
768 size of circles denotes the number of ambient monitoring sites of cities. In (b), the red  
769 capitals denote six typical polluted cities in NCP. A: Beijing; B: Tianjin; C:  
770 Shijiazhuang; D: Baoding; E: Tangshan; F: Chengde. The blue numbers denote the  
771 CERN sites with the hourly RH measurement. 1: Jiaozhouwan; 2: Yucheng; 3:  
772 Luancheng.
- 773 Figure 2 Scatter plots of near-surface  $[\text{PM}_{2.5}]$  and RH at six typical polluted cities in NCP  
774 during the 2015 wintertime. The red diamond shows the bin average of near-surface  
775  $[\text{PM}_{2.5}]$ , and the red line denotes the variation of the bin average of near-surface  
776  $[\text{PM}_{2.5}]$  with RH.
- 777 Figure 3 Comparison of measured (black dots) and predicted (red line) diurnal profiles of the  
778 RH in (a) Luancheng, (b) Yucheng, and (c) Jiaozhouwan from 05 December 2015 to  
779 04 January 2016.
- 780 Figure 4 Spatial distribution of (a) NCEP reanalyzed and (b) simulated RH averaged from 05  
781 December 2015 to 04 January 2016.
- 782 Figure 5 (a) absolute and (b) relative AOD contribution caused by the ALW, averaged from  
783 05 December 2015 to 04 January 2016.
- 784 Figure 6 Near-surface  $[\text{PM}_{2.5}]$  contribution caused by the ALW-ARF, averaged from 05  
785 December 2015 to 04 January 2016.
- 786 Figure 7 Average variations of AOD and Reff in  $f_{base}$  (red line) and  $f_{alw-rad0}$  (blue line)  
787 as a function of bin  $[\text{PM}_{2.5}]$  in NCP during daytime from 05 December 2015 to 04  
788 January 2016.
- 789 Figure 8 Average (a) percentage decrease of SWDOWN at the ground surface, (b) decrease of  
790 TSFC, (c) percentage decrease of PBLH, and (d) percentage contribution of  
791 near-surface  $[\text{PM}_{2.5}]$  caused by the ALW-ARF, as a function of the near-surface  $[\text{PM}_{2.5}]$   
792 in NCP during daytime from 05 December 2015 to 04 January 2016.
- 793 Figure 9 Average variations of daytime  $\text{NO}_2$  photolysis and  $\text{O}_3$  concentration at 1<sup>st</sup> and 5<sup>th</sup>  
794 model layer (around 18 m and 420 m above the ground surface, respectively) caused  
795 by ALW from 05 December 2015 to 04 January 2016 in NCP.
- 796 Figure 10 Near-surface  $\text{PM}_{2.5}$  contribution caused by the ALW-J, averaged from 05  
797 December 2015 to 04 January 2016 in NCP.
- 798 Figure 11 Near-surface sulfate, nitrate, and ammonium contribution caused by the ALW-HET,  
799 averaged from 05 December 2015 to 04 January 2016.
- 800 Figure 12 Spatial distribution of  $\text{NH}_3$  emission rate in December.
- 801 Figure 13 Near-surface SOA contribution caused by the ALW-HET, averaged from 05  
802 December 2015 to 04 January 2016.
- 803 Figure 14 Near-surface  $\text{PM}_{2.5}$  contribution caused by the ALW-HET, averaged from 05  
804 December 2015 to 04 January 2016.
- 805 Figure 15 Average percentage decrease of (a) BC and (b) POA concentrations caused by the



806 ALW-HET, as a function of the near-surface  $[PM_{2.5}]$  in NCP from 05 December 2015  
807 to 04 January 2016.

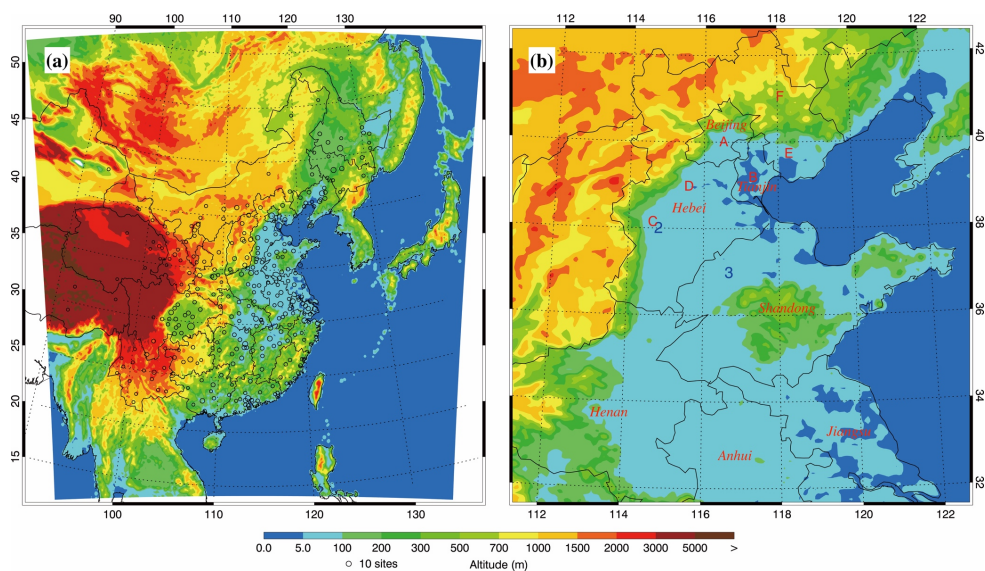
808 Figure 16 Average variations of (a) AOD and (b) Reff in  $f_{base}$  (red line) and  $f_{alw-het0}$   
809 (blue line), respectively, and average percentage decrease of near-surface (c) aerosol  
810 number concentration and (d) surface area caused by the ALW-HET, as a function of  
811 bin  $[PM_{2.5}]$  in NCP from 05 December 2015 to 04 January 2016.

812 Figure 17 Average (a) percentage decrease of SWDOWN at the ground surface, (b) decrease  
813 of TSFC, and (c) percentage decrease of PBLH caused by the ALW-HET, as a  
814 function of the near-surface  $[PM_{2.5}]$  in NCP during daytime from 05 December 2015  
815 to 04 January 2016.

816 Figure 18 Near-surface  $PM_{2.5}$  contribution caused by the ALW-TOT, averaged from 05  
817 December 2015 to 04 January 2016 in NCP.

818 Figure 19 Average contributions to near-surface  $[PM_{2.5}]$  caused by the ALW-TOT (black line),  
819 ALW-HET (red line), ALW-RAD (green line), and ALW-J (blue line), respectively, as  
820 a function of the RH in NCP from 05 December 2015 to 04 January 2016.

821  
822  
823  
824  
825



826

827

828 Figure 1 (a) WRF-CHEM simulation domain with topography and (b) North China Plain. In  
829 (a), the blue circles represent centers of cities with ambient monitoring sites and the size of  
830 blue circles denotes the number of ambient monitoring sites of cities. In (b), the red capitals  
831 denote six typical polluted cities in NCP. A: Beijing; B: Tianjin; C: Shijiazhuang; D: Baoding;  
832 E: Tangshan; F: Chengde. The blue numbers denote the CERN sites with the RH  
833 measurement. 1: Jiaozhouwan; 2: Yucheng; 3: Luancheng.

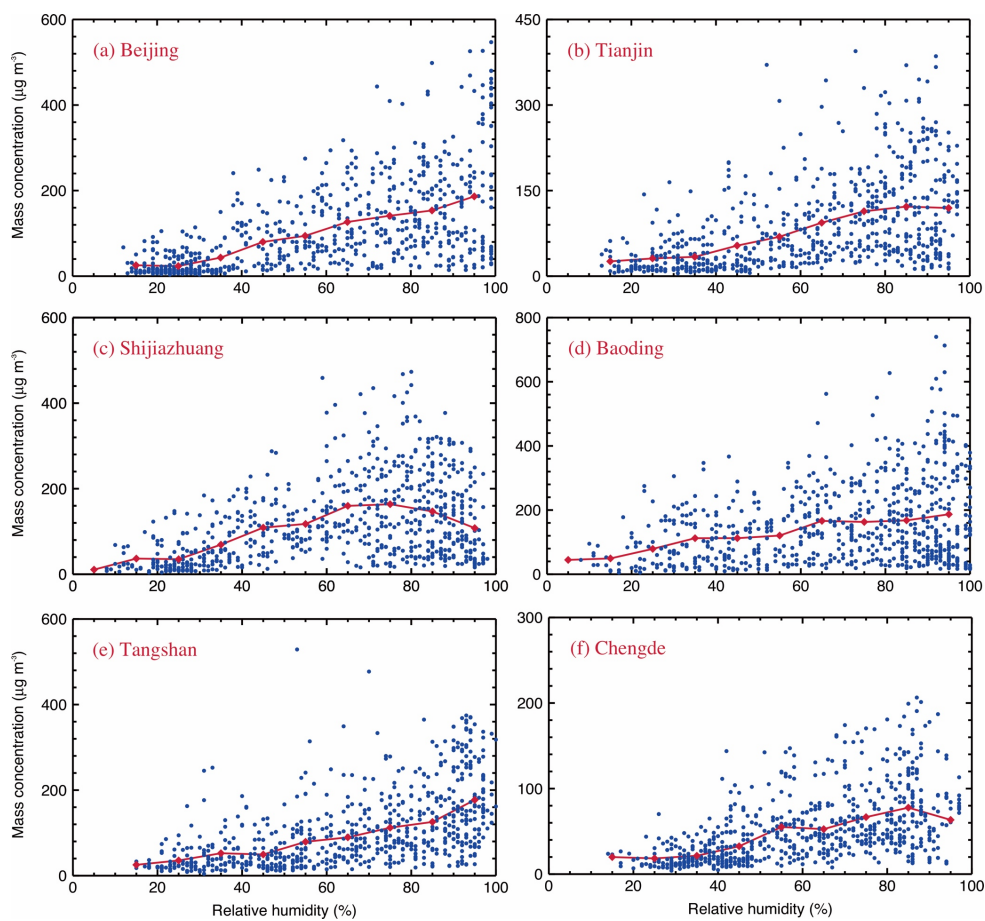
834

835

836

837

838



839

840

841 Figure 2 Scatter plots of near-surface  $[PM_{2.5}]$  and RH at six typical polluted cities in NCP  
842 during the 2015 wintertime. The red diamond shows the bin average of near-surface  $[PM_{2.5}]$ ,

843 and the red line denotes the variation of the bin average of near-surface  $[PM_{2.5}]$  with RH.

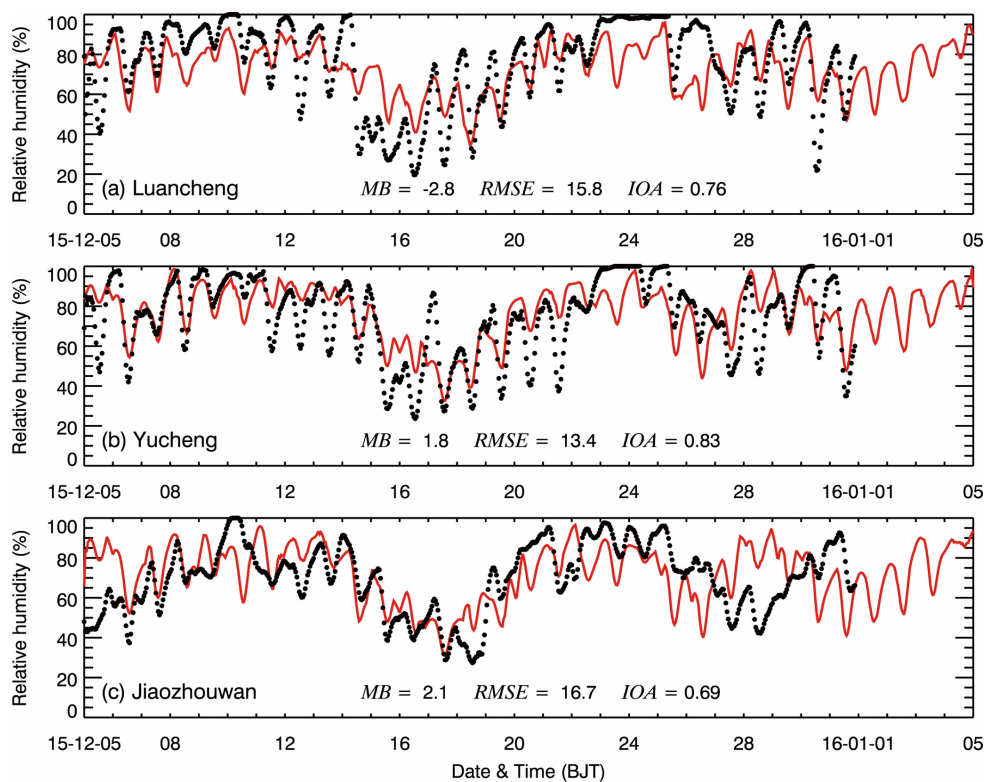
844

845

846

847

848



849

850

851 Figure 3 Comparison of measured (black dots) and predicted (red line) diurnal profiles of the

852 RH in (a) Luancheng, (b) Yucheng, and (c) Jiaozhouwan from 05 December 2015 to 04

853 January 2016.

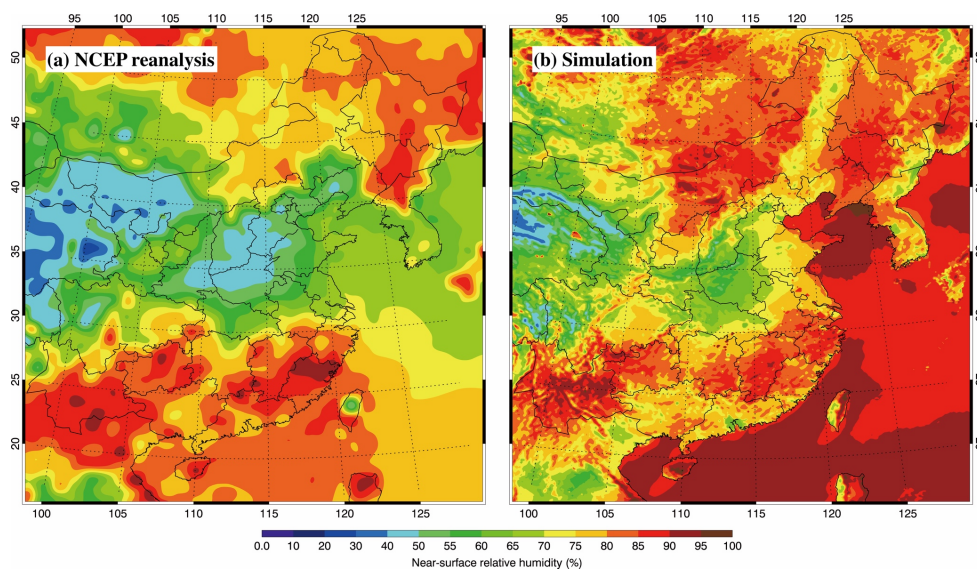
854

855

856

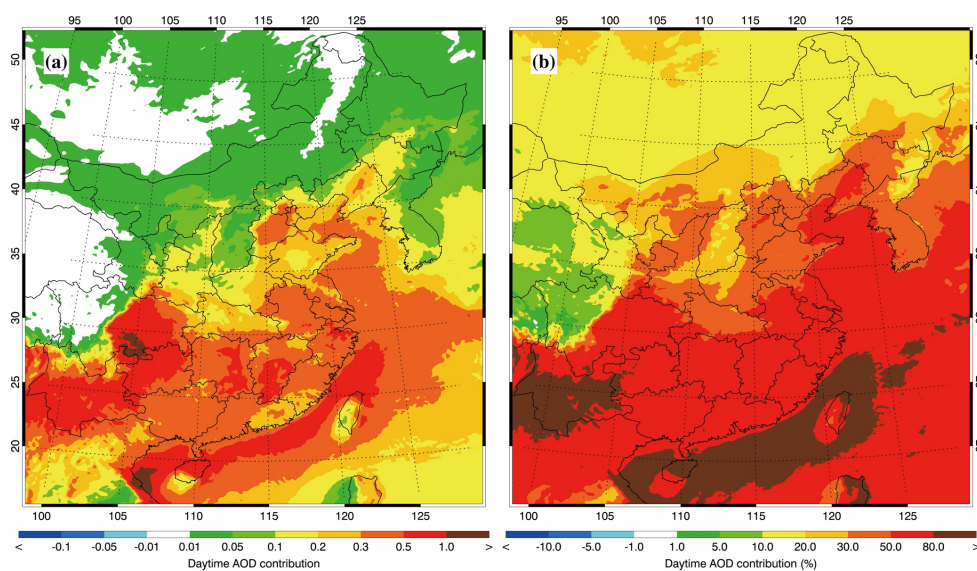
857

858



859  
860  
861  
862  
863  
864  
865  
866  
867

Figure 4 Spatial distribution of (a) NCEP reanalyzed and (b) simulated RH averaged from 05 December 2015 to 04 January 2016.



868

869

870 Figure 5 (a) absolute and (b) relative AOD contribution caused by the ALW, averaged from  
871 05 December 2015 to 04 January 2016.

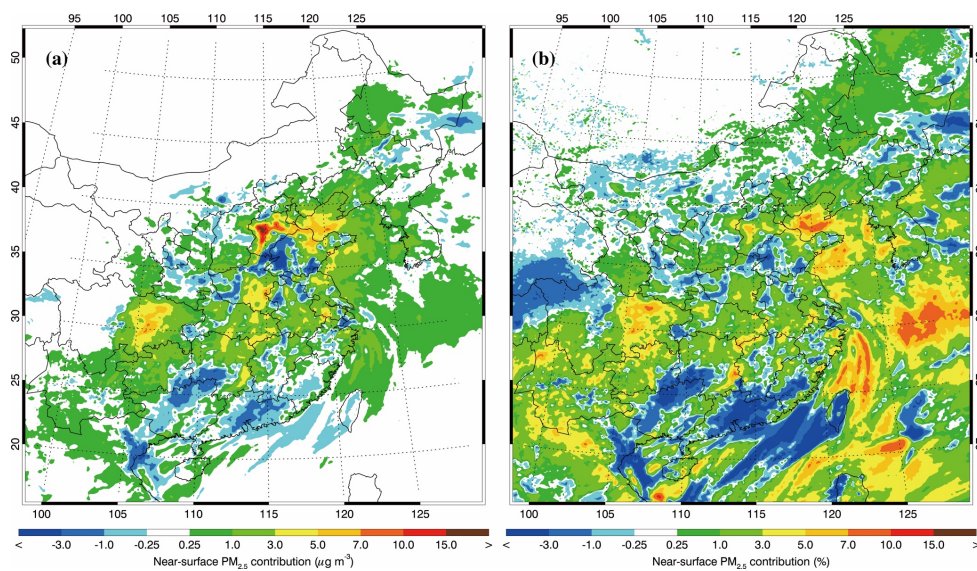
872

873

874

875

876



877

878

879 Figure 6 Near-surface PM<sub>2.5</sub> contribution caused by the ALW-ARF, averaged from 05

880 December 2015 to 04 January 2016 in NCP.

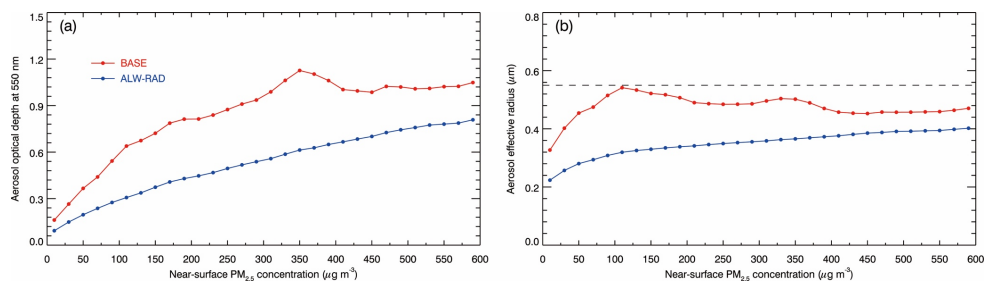
881

882

883

884

885



886

887

888 Figure 7 Average variations of AOD and Reff in  $f_{base}$  (red line) and  $f_{alw-rad0}$  (blue line)

889 as a function of bin  $[PM_{2.5}]$  in NCP during daytime from 05 December 2015 to 04 January

890 2016.

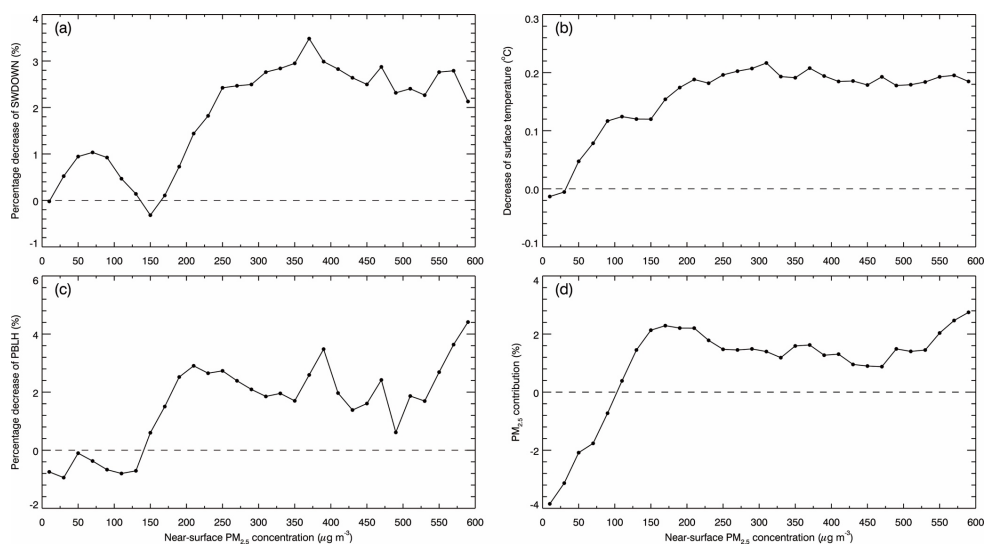
891

892

893

894

895



896

897

898 Figure 8 Average (a) percentage decrease of SWDOWN at the ground surface, (b) decrease of

899 TSFC, (c) percentage decrease of PBLH, and (d) percentage contribution of near-surface

900  $[PM_{2.5}]$  caused by the ALW-ARF, as a function of the near-surface  $[PM_{2.5}]$  in NCP during

901 daytime from 05 December 2015 to 04 January 2016.

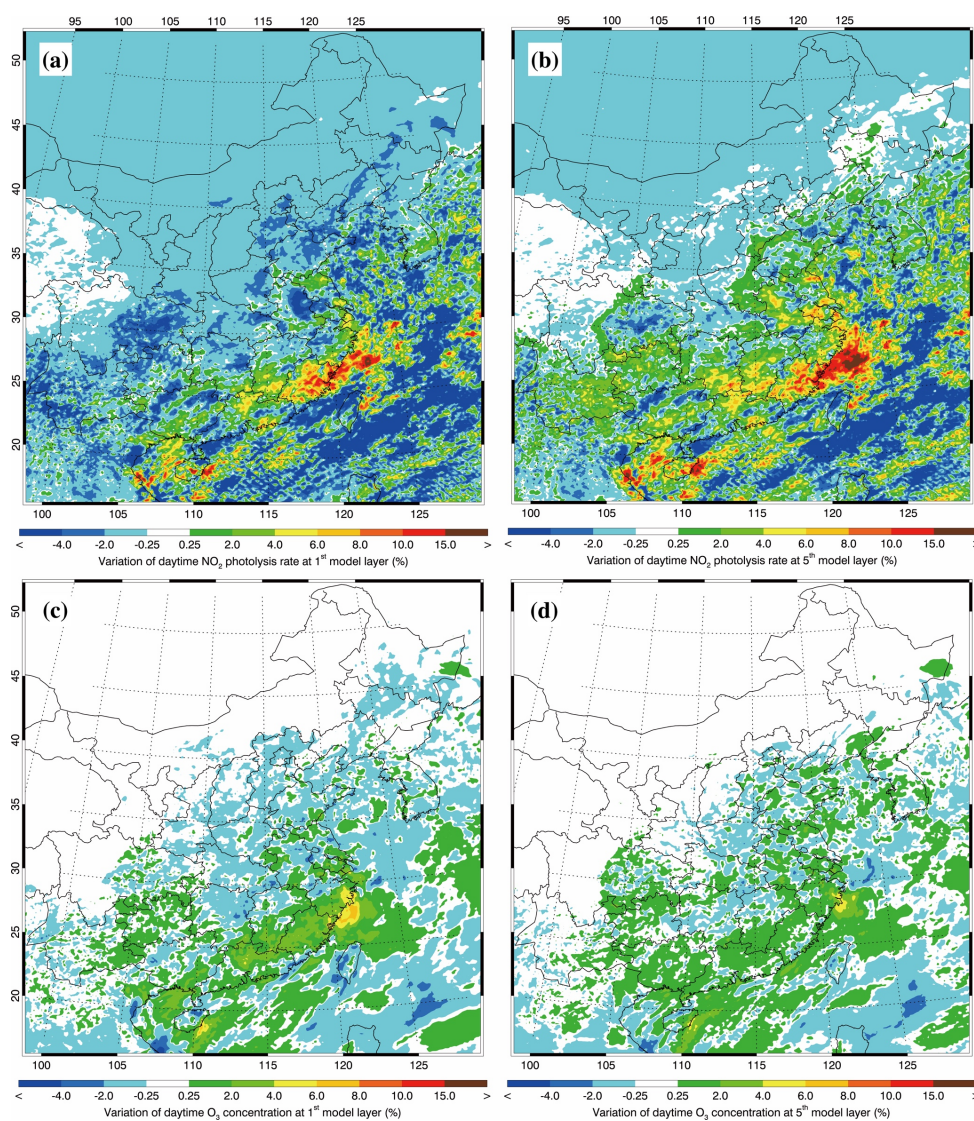
902

903

904

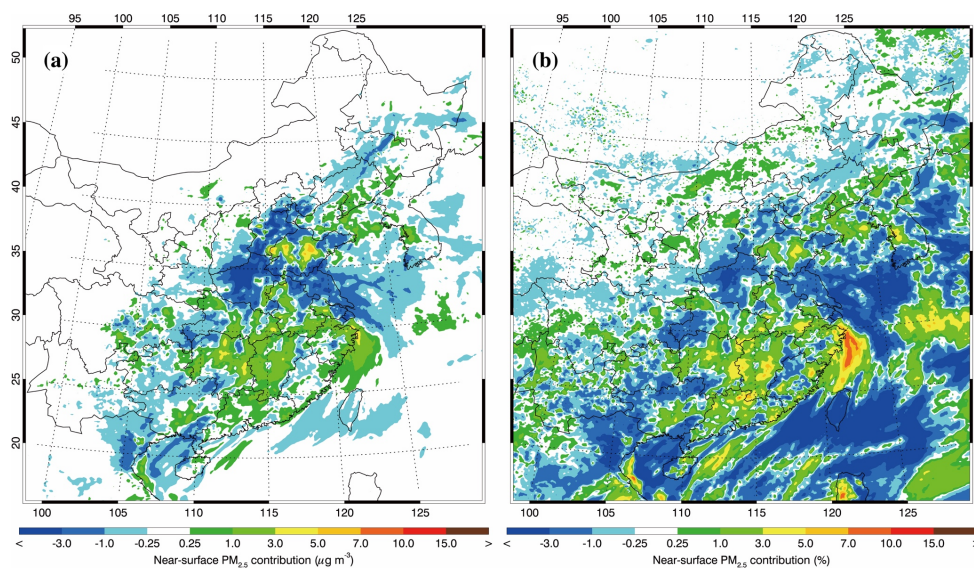
905

906



907  
908  
909  
910  
911  
912  
913  
914  
915  
916

Figure 9 Average variations of daytime NO<sub>2</sub> photolysis and O<sub>3</sub> concentration at 1<sup>st</sup> and 5<sup>th</sup> model layer (around 18 m and 420 m above the ground surface, respectively) caused by ALW from 05 December 2015 to 04 January 2016.



917

918

919 Figure 10 Near-surface PM<sub>2.5</sub> contribution caused by the ALW-J, averaged from 05

920 December 2015 to 04 January 2016.

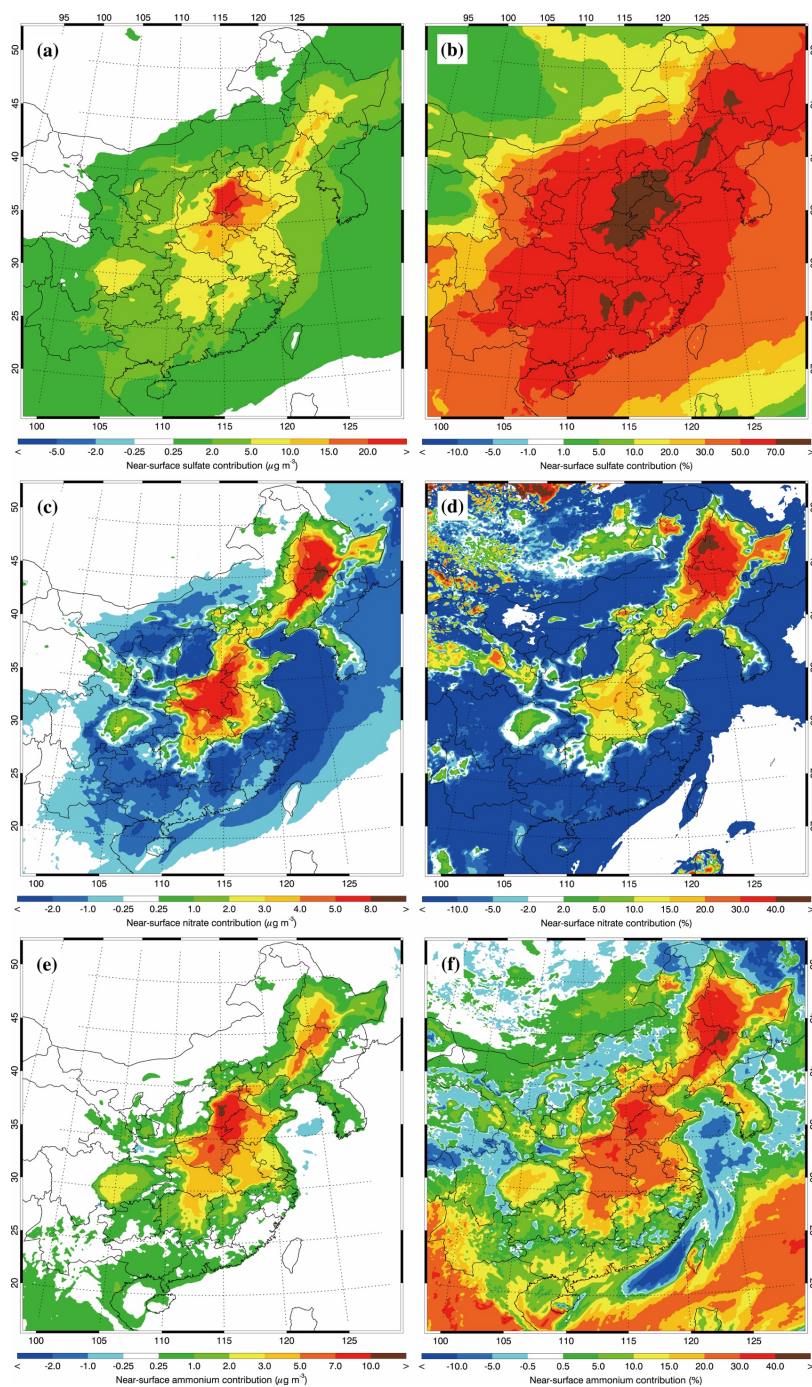
921

922

923

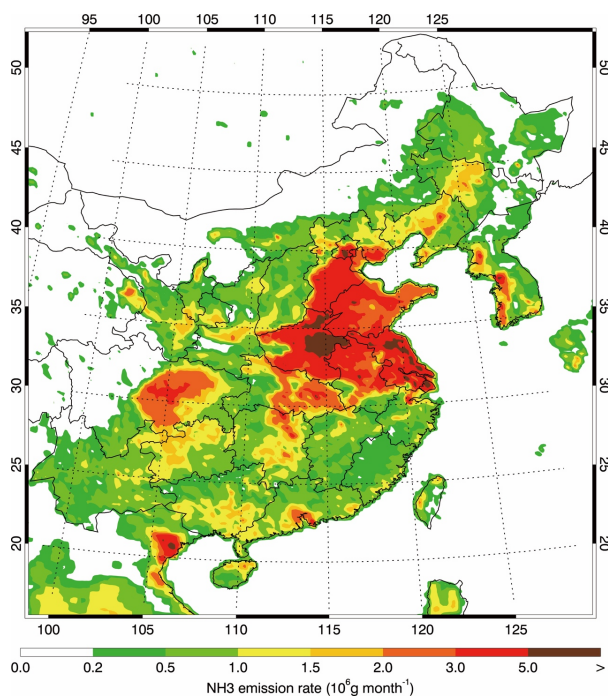
924

925



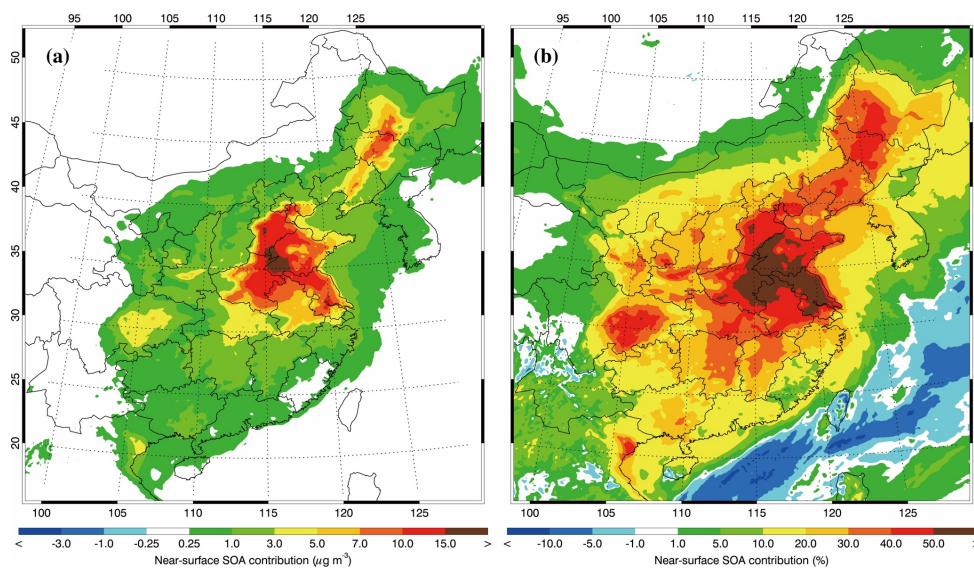
926  
927  
928  
929  
930

Figure 11 Near-surface sulfate, nitrate, and ammonium contribution caused by the ALW-HET, averaged from 05 December 2015 to 04 January 2016.



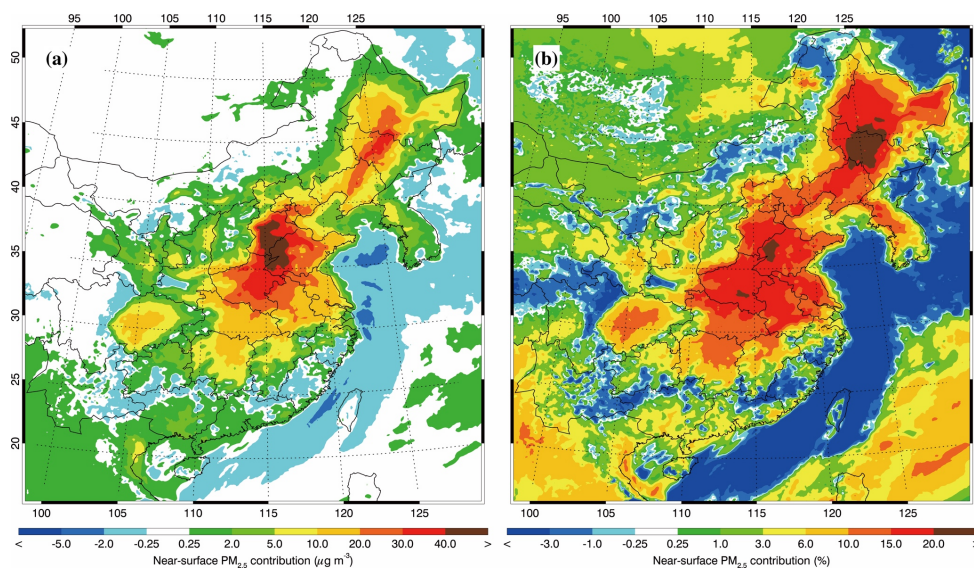
931  
932  
933  
934  
935  
936  
937  
938

Figure 12 Spatial distribution of NH<sub>3</sub> emission rate in December.



939  
940  
941  
942  
943  
944  
945  
946  
947

Figure 13 Near-surface SOA contribution caused by the ALW-HET, averaged from 05 December 2015 to 04 January 2016.



948

949

950 Figure 14 Near-surface [ $PM_{2.5}$ ] contribution caused by the ALW-HET, averaged from 05

951 December 2015 to 04 January 2016.

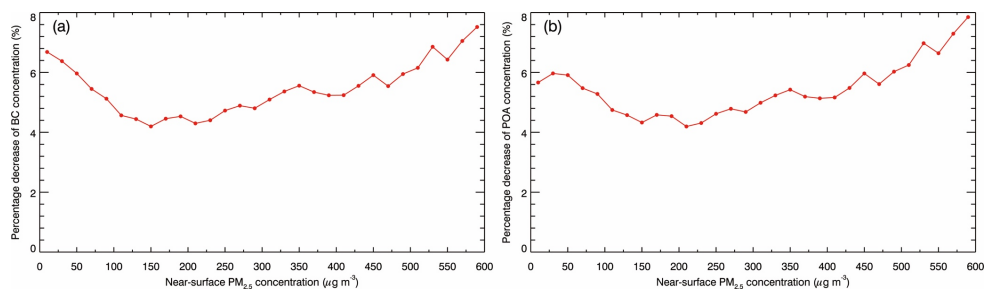
952

953

954

955

956



957

958

959 Figure 15 Average percentage decrease of (a) BC and (b) POA concentrations caused by the

960 ALW-HET, as a function of the near-surface [PM<sub>2.5</sub>] in NCP from 05 December 2015 to 04

961 January 2016.

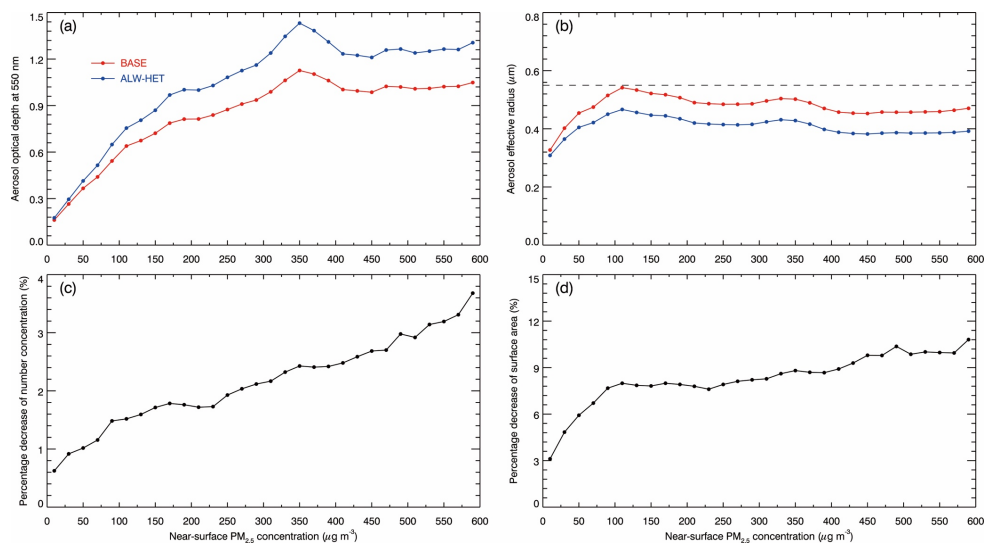
962

963

964

965

966



967

968

969 Figure 16 Average variations of (a) AOD and (b) Reff in  $f_{base}$  (red line) and  $f_{alw-het0}$

970 (blue line), respectively, and average percentage decrease of near-surface (c) aerosol number

971 concentration and (d) surface area caused by the ALW-HET, as a function of bin [PM<sub>2.5</sub>] in

972 NCP from 05 December 2015 to 04 January 2016.

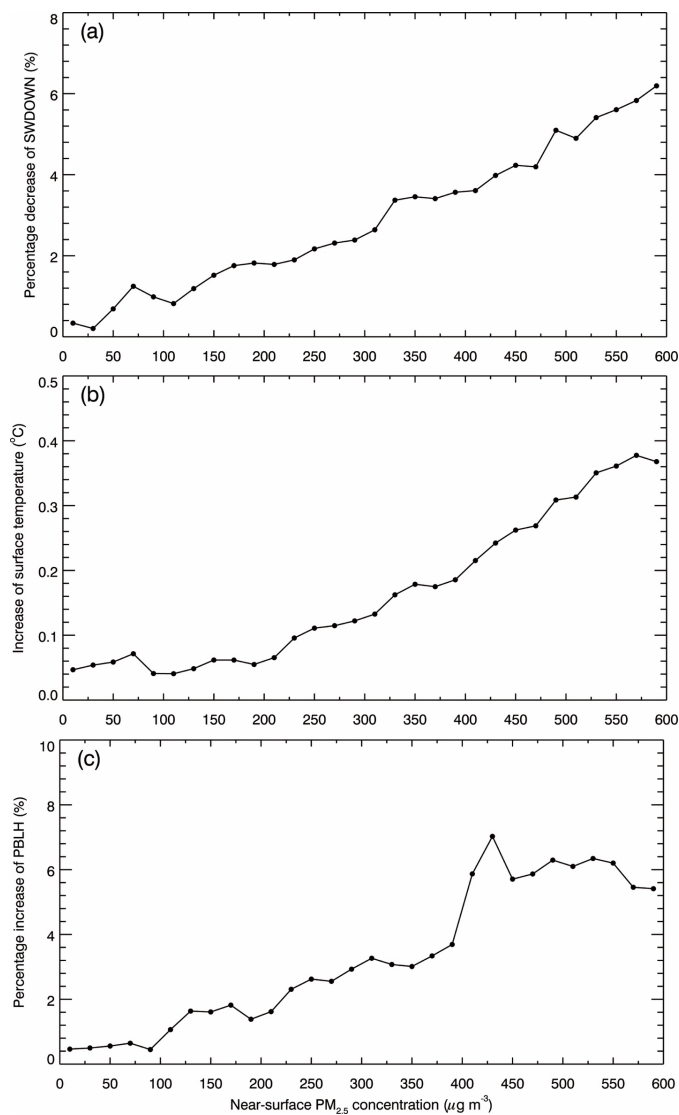
973

974

975

976

977



978

979

980

981

982

983

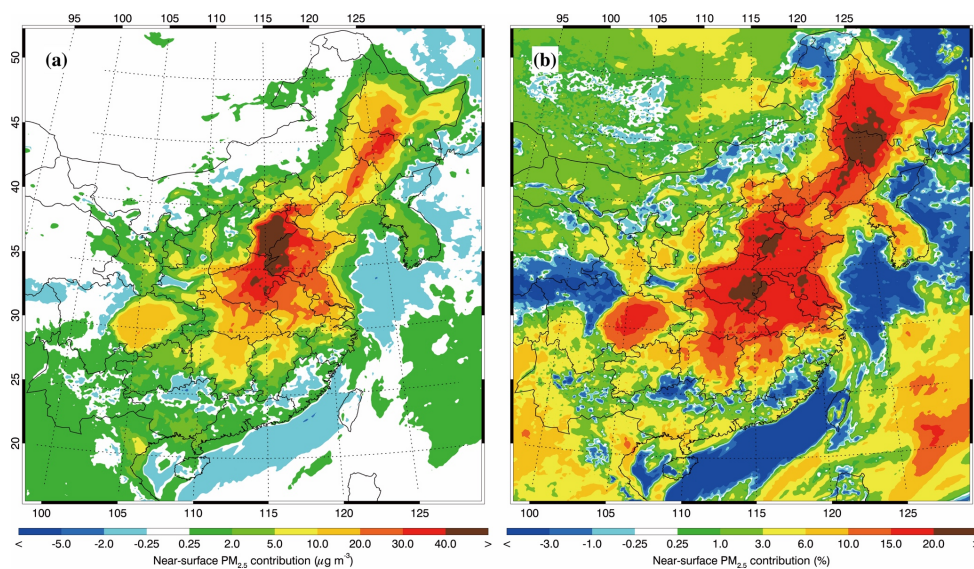
984

985

986

987

Figure 17 Average (a) percentage decrease of SWDOWN at the ground surface, (b) decrease of TSFC, and (c) percentage decrease of PBLH caused by the ALW-HET, as a function of the near-surface [PM<sub>2.5</sub>] in NCP during daytime from 05 December 2015 to 04 January 2016.



988

989

990 Figure 18 Near-surface PM<sub>2.5</sub> contribution caused by the ALW-TOT, averaged from 05

991 December 2015 to 04 January 2016.

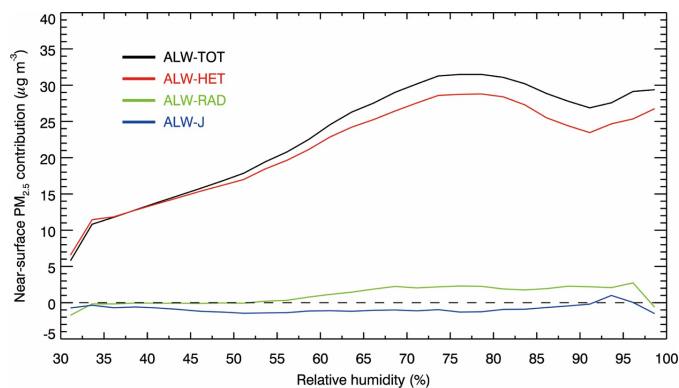
992

993

994

995

996



997

998

999 Figure 19 Average contributions to the near-surface [PM<sub>2.5</sub>] caused by the ALW-TOT (black  
1000 line), ALW-HET (red line), ALW-RAD (green line), and ALW-J (blue line), respectively, as a  
1001 function of the RH in NCP from 05 December 2015 to 04 January 2016.

1002

1003

1004

1005